

Unsupervised detection and classification of heartbeats using the dissimilarity matrix in PCG signals

J. Torre-Cruz ^{*a}, D. Martinez-Muñoz^a, N. Ruiz-Reyes^a, A.J. Muñoz-Montoro^b, M. Puentes-Chiachio^c, F.J. Canadas-Quesada^a

^aDepartment of Telecommunication Engineering, University of Jaen, Campus Científico-Tecnológico de Linares, Avda. de la Universidad, s/n, 23700 Linares, Jaen, Spain

^bDepartment of Computer Science, University of Oviedo, Campus de Gijón, s/n, Gijón, 33203, Spain

^cCardiology, University Hospital of Jaen, Av. del Ejercito Espanol, 10, 23007 Jaen, Spain

Abstract

Background and objective: Auscultation is the first technique applied to the early diagnose of any cardiovascular disease (CVD) in rural areas and poor-resources countries because of its low cost and non-invasiveness. However, it highly depends on the physician's expertise to recognize specific heart sounds heard through the stethoscope. The analysis of phonocardiogram (PCG) signals attempts to segment each cardiac cycle into the four cardiac states (S1, systole, S2 and diastole) in order to develop automatic systems applied to an efficient and reliable detection and classification of heartbeats. In this work, we propose an unsupervised approach, based on time-frequency characteristics shown by cardiac sounds, to detect and classify heartbeats S1 and S2. *Methods:* The proposed system consists of a two-stage cascade. The first stage performs a rough heartbeat detection while the second stage refines the previous one, improving the temporal localization and also classifying the heartbeats into types S1 and S2. The first contribution is a novel approach that combines the dissimilarity matrix with the frame-level spectral divergence to locate heartbeats using the repetitiveness shown by the heart sounds and the temporal relationships between the intervals defined by the events S1/S2 and non-S1/S2 (systole and diastole). The second contribution is a verification-correction-classification process based on a sliding window that allows the preservation of the temporal structure of the cardiac cycle in order to be applied in the heart sound classification. The proposed method has been assessed using the open access databases PASCAL, CirCor DigiScope Phonocardiogram and an additional sound mixing procedure considering both Additive White Gaussian Noise (AWGN) and different kinds of clinical ambient noises from a commercial database. *Results:* The proposed method outperforms the detection and classification performance of other recent state-of-the-art methods. Although our proposal achieves the best average accuracy for PCG signals without cardiac abnormalities, 99.4% in heartbeat detection and 97.2% in heartbeat classification, its worst average accuracy is always above 92% for PCG signals with cardiac abnormalities, signifying an improvement in heartbeat detection/classification above 10% compared to the other state-of-the-art methods evaluated. *Conclusions:* The proposed method provides the best detection/classification performance in realistic scenarios where the presence of cardiac anomalies as well as different types of clinical environmental noises are active in the PCG signal. Of note, the promising modelling of the temporal structures of the heart provided by the dissimilarity matrix together with the frame-level spectral divergence, as well as the removal of a significant number of spurious heart events and recovery of missing heart events, both corrected by the proposed verification-correction-classification algorithm, suggest that our proposal is a successful tool to be applied in heart segmentation.

Keywords: Phonocardiography, unsupervised, detection/classification, heartbeat S1/S2, dissimilarity, divergence.

*Corresponding author. Tlf.: (+34) 953648592

Email address: jtorre@ujaen.es (J. Torre-Cruz *)

1. Introduction

The World Health Organization (WHO) reports that cardiovascular diseases (CVDs), such as heart failure, are among the leading causes of death worldwide, claiming approximately 18 million lives each year [1]. In Spain, more than 125,000 people die each year from CVDs, with around 315 acute myocardial infarctions per 100,000 male inhabitants and 80 per 100,000 female inhabitants, with an annual increase of 2% in the occurrence of non-fatal infarctions within the male population [2]. Due to the seriousness of this situation, the European Commission is building the Horizon Europe's Strategic Plan 2021-2024 in order to achieve an improved evidence-based health policies, and more effective solutions for health promotion and disease prevention [3]. Thus, most research efforts of the biomedical signal processing community are being focused on early identifying people at increased risk of developing CVDs in order to accelerate the application of medical treatment to prevent premature death, since WHO specifies that 80% of both premature heart diseases and strokes are preventable [4].

From a physiological standpoint, a normal heart rate (HR) can be defined as a repetitive sequence of two primary heart sounds, S1 (known as lub) and S2 (known as dub), during each heart cycle [5]. The sounds S1 and S2 follow specific temporal-spectral patterns, given that the HR associated to an adult person ranges between 60-80 beats per minute (bpm) and can be considered a predictor of cardiovascular risk whenever a resting HR is above 80 bpm [6]. In fact, both the HR and the spectral content associated to heart sounds can reveal useful medical information on cardiovascular risk, being the continuous HR monitoring most important for the early diagnosis of CVDs [7]. It is well known that S1 occurs at systole phase, closing the mitral and tricuspid valves, while S2 occurs at diastole phase, closing the aortic and pulmonic valves. Although most of the time it is assumed that systole is shorter than diastole [8, 9, 10], the duration of systole is commonly considered relatively constant [11, 12, 13] whereas the length of diastole varies according to the HR [14, 12]. Comparing S1 and S2, S1 usually shows a low-pitch (about 20-150 Hz) with an average longer duration (about 70-160 ms) and higher amplitude. However, S2 often shows a high-pitch (about 20-200 Hz) sound with an average shorter duration (about 60-140 ms) and lower amplitude [15, 16, 13]. In unhealthy adults, in addition to the primary heart sounds S1 and S2, there are also abnormal heart sounds such as murmurs characterised by the concentration of most of their energy in the spectral range of 15-700 Hz and normally located within the systole or diastole [13, 16].

Techniques such as echocardiography, electrocardiography (ECG) or medical resonance imaging (MRI) are usually used to diagnose CVDs, however, these techniques involve a higher cost compared to auscultation, so it is difficult for these techniques to be applied in low- and middle-income countries as it is not an economically viable option. Alternatively, auscultation can diagnose effectively CVDs [17] and it remains the most commonly applied technique in poor-resources countries to early diagnose any CVD because of its low cost, non-invasiveness and user-friendliness. Nevertheless, the reliability of this technique highly depends on the human auditory system, the sound quality captured by the stethoscope and the physician's expertise in order to recognize and interpret the meaning of the sounds heard through the medical devices [17, 18]. As a consequence, the analysis of heart sounds by phonocardiography (PCG) has become a research topic of high interest in the biomedical signal processing community in recent years, since a PCG signal is a recording of heart sounds through the cardiac cycles by means of a digital stethoscope or microphone mainly located over the chest wall of the patient [15], as shown in Figure 1. PCG signal analysis, in addition to providing the HR and duration of systole and diastole as does ECG, can extract additional information (e.g. energy distribution and spectral envelope of heart sounds in the time-frequency domains) of high interest to medical professionals and engineers, because it is best suited to further analyse both normal and abnormal heart sounds.

Focusing on PCG signals, the first task is usually the HR estimation, however, it is highly associated with heart segmentation [20]. The aim of the heart segmentation (HS) in the PCG signal is twofold: i) localization of frames in which the heart sounds are active and, ii) classification of the previous cardiac frames into S1 and S2 [5, 7]. As a result, the four states of each heart cycle are defined: S1, S2, systole (time interval between S1 and S2), diastole (time interval between S2 and S1) [21] and the HR, implicitly. Therefore, the accurate temporal localization of this sequence of repetitive S1 and S2 heart sounds is the key [22, 17] to developing any heart sound detection [23, 24, 7] [25, 26] or classification system [7, 25, 26, 27, 28, 29], since

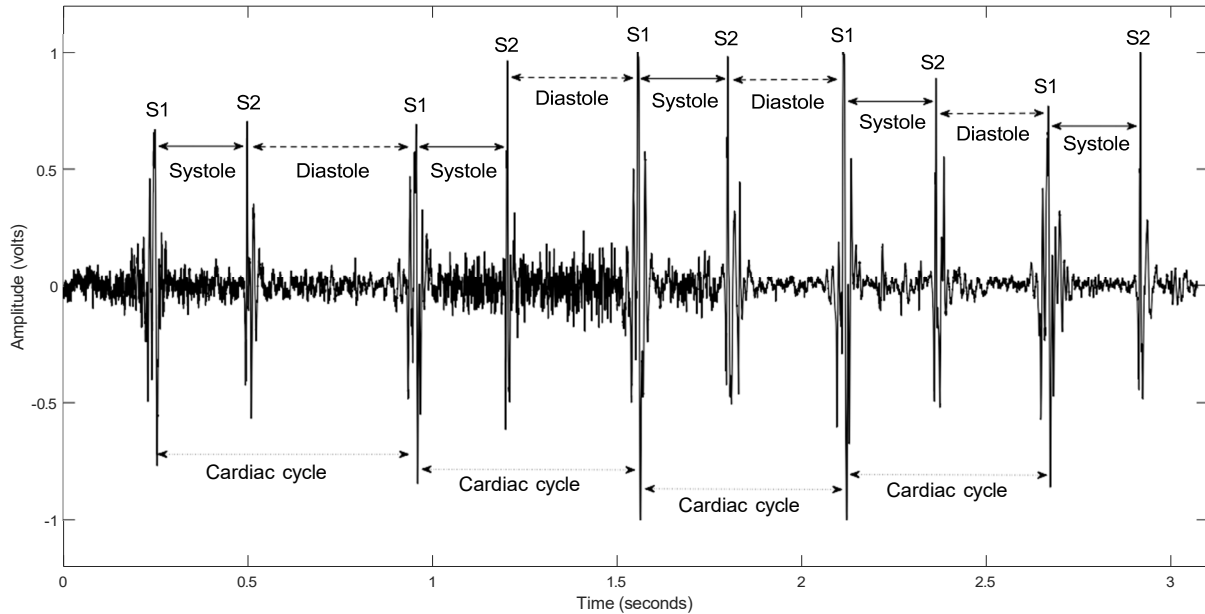


Figure 1: An example of PCG signal, obtained from database PASCAL (173_1307973611151_C.wav) [19], with annotations of the parts that compose each cardiac cycle. It can be observed that the duration of systole is approximately the same in each cardiac cycle but this is not the case when the diastole is analysed.

52 their performances highly depend on the accuracy obtained in the segmentation stage, in order to extract
 53 and classify specific time-frequency features.

54 Focusing on the temporal repeatability shown by specific sounds in the real-world, temporal regularity
 55 plays a facilitating role in pattern detection according to [30, 31]. The human auditory system can easily
 56 isolate those sounds by identifying them as repeating patterns active in the input signal as occurs with the
 57 soloist and rhythmic accompaniment in a musical sound context. In the last years, many signal processing
 58 approaches have been proposed in order to exploit the temporal repeatability of sounds in different research
 59 fields, such as audio [32, 33, 34], image [35] and biomedicine [36, 18]. Specifically, the concept of self-
 60 similarity was initially proposed to visualise the time structure of music [37] and later to extract the repeating
 61 background from the foreground in musical signals but authors aimed that it could be generalised to any kind
 62 of repeating patterns because the similarity information showed a high robustness to successfully extract
 63 intermittent or variable periods from a repeating structure [33]. With this in mind, it would be interesting
 64 to explore the event detection and classification applied to heart sounds using the previously mentioned
 65 similarity information since the heart sounds are widely considered the most intuitive and repetitive pattern
 66 in the human nature [38] [39].

67 In literature, numerous heart segmentation works have been proposed in the last decades, being the most
 68 common approaches categorised in Fourier transform [40, 41], envelope-based [42, 43], wavelet [44, 45, 46],
 69 energy-based [47, 38, 48, 23, 49], S-transform [43, 39], Support vector machine (SVM) [50, 51], Spectral
 70 clustering [25], Hidden markov model (HMM) [52, 53], empirical mode decomposition [54, 55], Homomorphic
 71 filtering [56, 7], Neural networks [22, 17, 9, 57] and Mel-frequency cepstral coefficients (MFCC) [47, 26].
 72 Authors [46] detailed a novel method for detecting and classifying heart sounds and murmurs by means
 73 of empirical wavelet transform-based PCG signal decomposition, the Shannon entropy envelope extraction,
 74 the instantaneous phase-based boundary determination, heart sound and murmur parameter extraction,
 75 the systole/diastole discrimination and the decision rules-based murmur classification. Mubarak et al. [7]
 76 proposed the concept of quality assessment before localization, feature extraction and classification of heart
 77 sounds. Specifically, the signal quality is assessed by predefined criteria based upon the number of peaks
 78 and zero crossing of the PCG signal. Once quality assessment is performed, then heart beats within the

79 PCG signal are localised, which is done by envelope extraction using homomorphic envelopogram and finding
80 prominent peaks. In order to classify localised peaks into S1 and S2, temporal and time-frequency based
81 statistical features have been used. Support Vector Machine using radial basis function kernel is used for
82 classification of heart beats into S1 and S2 based upon extracted features. In [9], a convolutional network
83 architecture, inspired by a network used for image segmentation, was combined with a sequential temporal
84 modeling procedure in order to provide segmentation results compatible with the sequential nature of heart
85 sounds. Convolutional Neural Network (CNNs) were also incorporated in segmentation algorithms using
86 HMMs. Results showed that CNNs improved performance in recovering the exact positions of fundamental
87 heart sounds in PCGs. According to [25], an unsupervised approach to detect the positions of heart sound
88 events S1 and S2 in PCGs recordings is presented. Gammatone filter bank features and a spectral clustering
89 technique were used for the segmentation of S1/S2 and non-S1/S2 heart sound events. In [57], a real-time
90 algorithm for heart segmentation based on CNN is developed testing feature extraction methods using the
91 spectrum, envelopes, and 1D-CNN. Moreover, this approach is combined with the Viterbi algorithm to
92 correct the heart sound state order errors in the point-by-point classification algorithm. In [26], a complete
93 algorithm for automatic heartbeat detection and disorder discrimination is presented separating S1 and S2
94 by means of a power threshold, being the frame duration dynamically estimated according to the duration
95 of the sound S1 or S2. Lastly, two methods to combine MFCC estimates are proposed.

96 In this paper, we aim to develop an unsupervised detection and classification of S1 and S2 heartbeat
97 sounds combining the frame-level spectral divergence from the dissimilarity matrix applied to PCG record-
98 ings. In a first stage, an initial heart sound detection is estimated assuming both the well known repeatability
99 shown by the heartbeats and the additional temporal constraints among S1, S2, systole and diastole. In a
100 second stage, a more accurate detection is achieved improving the previous estimation and the classification
101 between S1 and S2 heartbeats is obtained using temporal assumptions between the systole and diastole.

102 The rest of the paper is organised as follows: the proposed method for detecting and classifying S1 and
103 S2 heartbeat sounds is detailed in Section 2. Section 3 describes the dataset, metrics, setup, the state-of-
104 the-art methods and results. The performance of the proposed method is discussed in Section 4. Finally,
105 conclusions and future work are presented in Section 5.

106 2. Proposed method

107 From the PCG signal $x[m]$ captured by a digital device (e.g., stethoscope or microphone), the goal of
108 the proposed method is to detect and classify the heart sounds S1 and S2. In this respect, we propose
109 an unsupervised approach based on the time-frequency characteristics of heartbeats to model the typical
110 behaviour of the heart sounds S1 and S2. As can be observed in Figure 2, the proposed method is composed
111 of two stages: Rough heartbeat detection (Stage I) and Fine heartbeat detection (Stage II). Briefly, Stage
112 I performs a preliminary heartbeat detection based on temporal repeatability of the heart sounds S1 and
113 S2 and the temporal relationships among heartbeats (S1 and S2) and the intervals between them (systole
114 and diastole). On the other hand, Stage II refines the temporal localization of the heartbeats detected in
115 the previous stage and classifies them into S1 or S2, assuming temporal relationships between systole and
116 diastole.

117 2.1. Stage I. Rough heartbeat detection

118 The objective of this stage is to obtain an approximate detection of the heartbeats S1 and S2, assuming
119 the following two common temporal-spectral behaviours observed in most heart sounds: i) heart sounds can
120 be modelled as spectral structures that repeat over time, showing similar frequency patterns between S1
121 and S2 but distinct from those patterns that can be found in systole and diastole [25]; and ii) the duration
122 of both S1 and S2 is shorter than systole and diastole [15]. Based on the two cardiac behaviors mentioned
123 above, we propose the dissimilarity matrix, a novel modification of the standard similarity matrix [33], that
124 exploits the above typical behaviors shown by most heart sounds. Specifically, this stage is divided into
125 three steps which are detailed below.

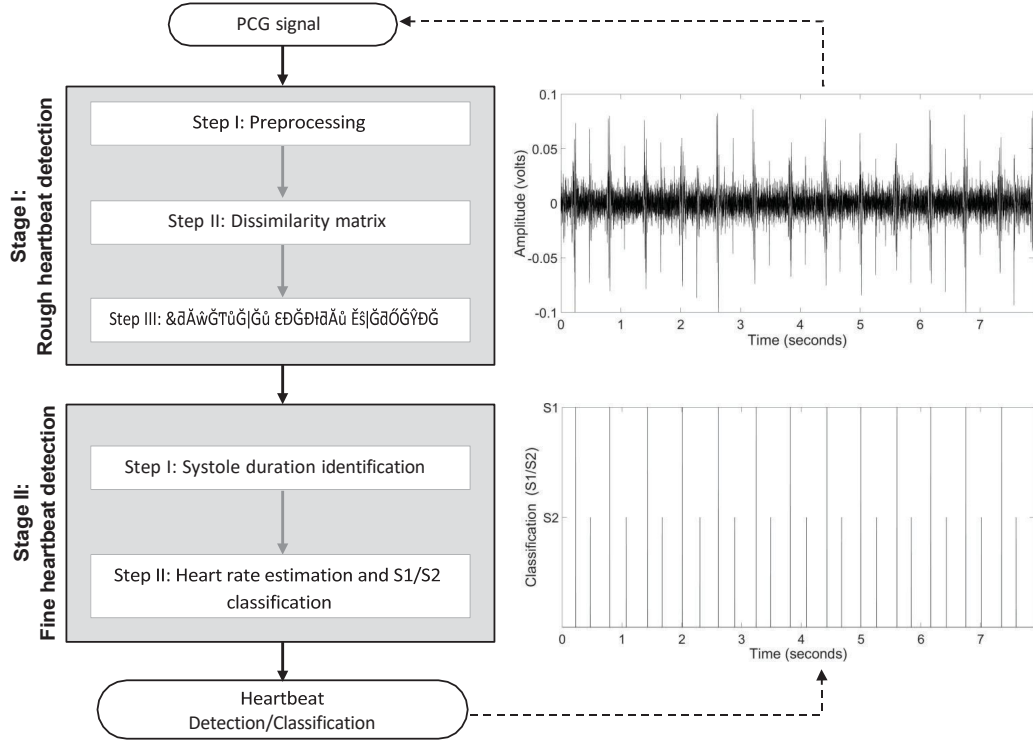


Figure 2: Block diagram of the proposed method.

2.1.1. Step I: Preprocessing

The magnitude spectrogram \mathbf{X} associated with the input PCG signal $x[m]$ is obtained applying the Short-Time Fourier Transform (STFT) with a Hamming windows of N samples and S , in percentage, overlap in order to analyse the spectral content shown by heart sounds. Each magnitude spectrogram \mathbf{X} is composed of T frames, F frequency bins and a set of time-frequency units $X_{f,t}$, being $f = 1, \dots, F$ and $t = 1, \dots, T$. Specifically, each unit $X_{f,t}$ represents the f^{th} frequency bin at the t^{th} frame. Moreover, \mathbf{X} is normalised to achieve independence both in size and scale and as result its energy equals 1.0. Thus, the normalised magnitude spectrogram $\bar{\mathbf{X}}$ is computed in Equation (1).

$$\bar{\mathbf{X}} = \frac{\mathbf{X}}{\sqrt{\sum_{f=1}^F \sum_{t=1}^T X_{f,t}^2}} \quad (1)$$

Next, a band-pass filter with cut-off frequencies from 20 to 200 Hz is applied to the normalised magnitude spectrogram $\bar{\mathbf{X}}$ to focus the analysis on the spectral structures of the heart sounds since it is well known that most of the energy of the sounds S1 and S2 is concentrated within the bandwidth 20 Hz to 200 Hz [15, 16, 13]. Note that to avoid complex nomenclature throughout the paper, the variable \mathbf{X} is hereinafter referred to the filtered version of the previous normalised magnitude spectrogram $\bar{\mathbf{X}}$. Figure 3 shows an example of PCG signal and its filtered spectrogram. It can be observed that the heart sounds show a repetitive structure over time, showing significant similarity among their spectral patterns across all cardiac cycles. Specifically, the spectral patterns related to S1 and S2 share similar time-frequency content, as well as the spectral patterns of beat-to-beat separation intervals such as systole and diastole. Moreover, the duration of S1 and S2 is always shorter compared to systole and diastole. It should be indicated to the reader that the recording analyzed in Figure 3 will be used throughout section 2 to explain the procedure applied for each step of the proposed method.

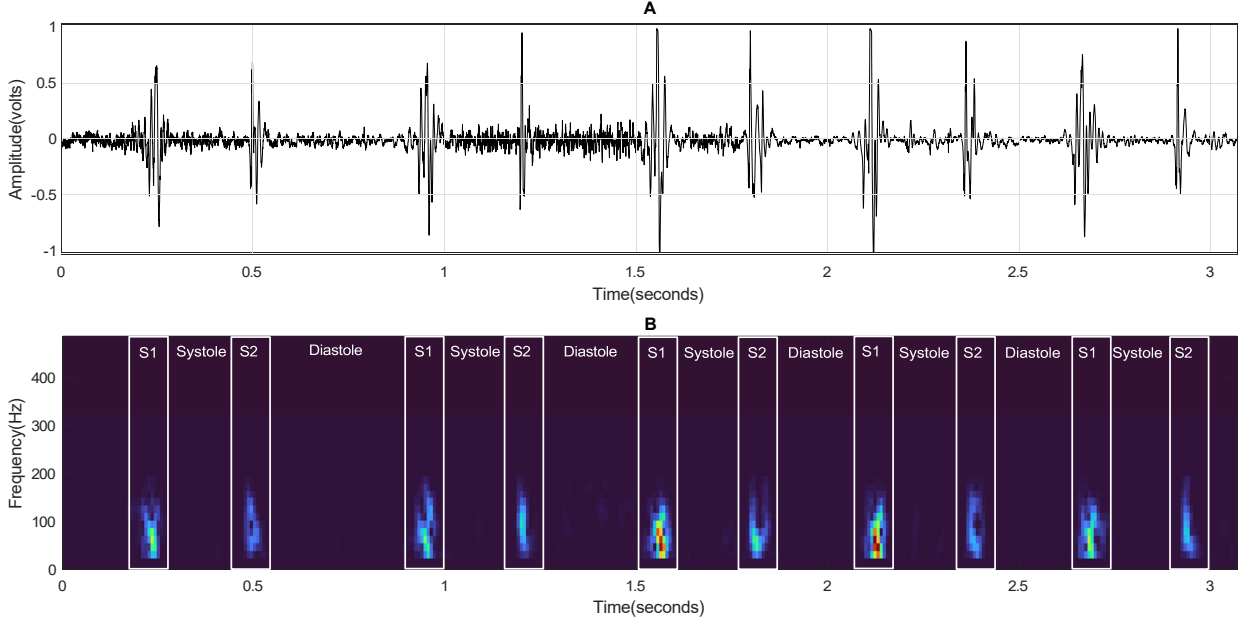


Figure 3: Example of recording "173_1307973611151_C.wav" obtained from database PASCAL [19]. A) Input PCG signal $x[m]$. B) Filtered spectrogram \mathbf{X} in which the annotations of the four states (S1, S2, systole and diastole) that compose each cardiac cycle are shown.

146 2.1.2. Step II: Dissimilarity matrix

147 In order to extract the repetitive structure shown by heart sounds from the PCG spectrogram \mathbf{X} , and
 148 thus locate in time the occurrence of the patterns S1 and S2, we propose the dissimilarity matrix \mathbf{D} as a
 149 new version of the standard similarity matrix [33] particularly adapted to heart sounds.

150 The dissimilarity matrix \mathbf{D} is a two-dimensional representation where each point $D_{i,j}$ measures the
 151 spectral dissimilarity between two frames X_i and X_j of the input PCG spectrogram \mathbf{X} , where $i = 1, \dots, T$
 152 and $j = 1, \dots, T$. In other words, the higher the dissimilarity between the spectral content of two frames, the
 153 higher the dissimilarity value and vice versa. The dissimilarity matrix obtains their minimum values in the
 154 main diagonal $D_{i,i}$ because each i^{th} frame is always the most similar to itself at any time. In general terms,
 155 the row or column i^{th} belonging to the matrix \mathbf{D} provides the degree of dissimilarity of the i^{th} frame with all
 156 frames that compose the spectrogram \mathbf{X} . In this paper, we propose to use the Kullback-Leibler divergence
 157 $d_{KL}(X_i|X_j)$ to provide the degree of dissimilarity between each frame pair $(X_i|X_j)$ of the spectrogram \mathbf{X}
 158 since $d_{KL}(X_i|X_j)$ provides a scale-invariant dissimilarity, and as a result, low energy sound components
 159 of X_i and X_j bear the same relative importance as high energy ones. The calculation of the dissimilarity
 160 matrix \mathbf{D} is shown in Equation (2).

$$D_{i,j} = d_{KL}(X_i|X_j) = \sum_{f=1}^F X_{f,i} \log \frac{X_{f,i}}{X_{f,j}} - X_{f,i} + X_{f,j} \quad \forall i, j \in [1, T] \quad (2)$$

161 In this paper, an event S1/S2 means a heartbeat sound of type S1 or S2, but we do not know to which of
 162 the two it belongs. As previously mentioned, the temporal information provided by the dissimilarity matrix
 163 \mathbf{D} could be useful to discriminate between spectral content belonging to heartbeats S1/S2 and beat-to-beat
 164 separation intervals, that is, diastole/systole. More specifically, those frames S1/S2 show a high degree of
 165 dissimilarity compared to those ones associated to systole/diastole, but a low degree of dissimilarity compared
 166 to other frames S1/S2 related to other heartbeats located at any time. Likewise, frames systole/diastole
 167 report a high degree of dissimilarity with frames S1/S2, but a low degree of dissimilarity compared to other
 168 frames belonging to systole/diastole. These facts can be observed in Figure 4.

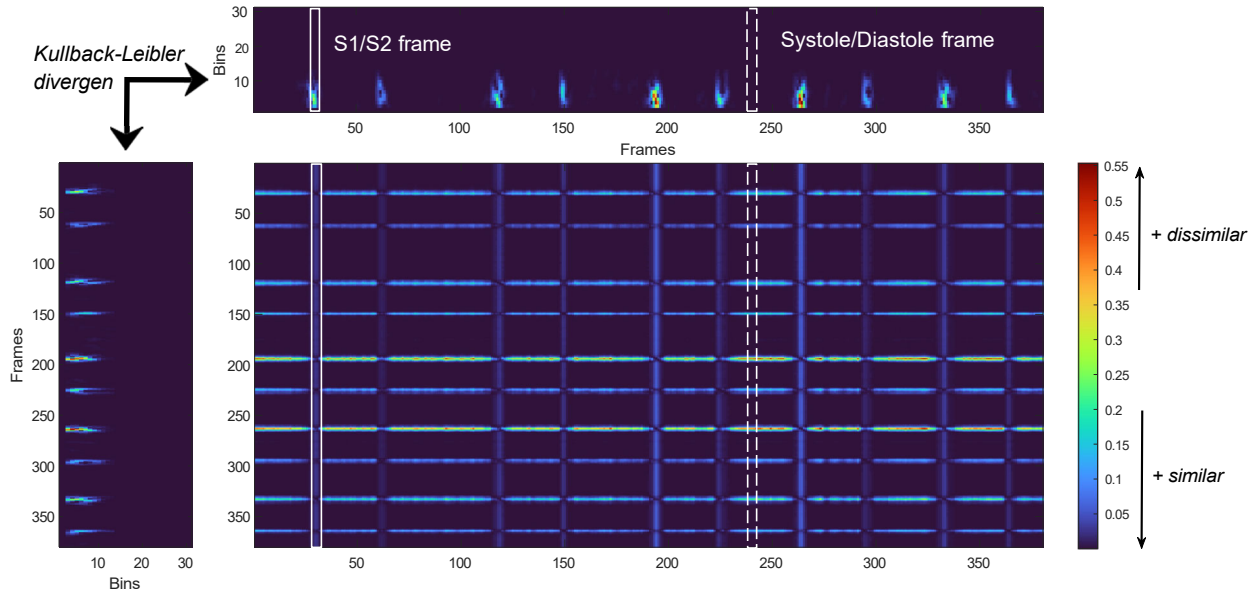


Figure 4: Example of recording "173_1307973611151 C.wav" from the database PASCAL [19]. The top and left subfigures show the filtered spectrogram \mathbf{X} of the input PCG signal. The middle subfigure shows the dissimilarity matrix \mathbf{D} , where each point $D_{i,j}$ measures the Kullback-Leibler divergence $d_{KL}(X_i|X_j)$ between two frames X_i and X_j of the spectrogram \mathbf{X} . The continuous white rectangle marks column 36 of matrix \mathbf{D} , showing the values of the Kullback-Leibler divergence between the frame X_{36} (frame S1/S2) and each frame of spectrogram \mathbf{X} , i.e., $d_{KL}(X_{36}|X_j)$ where $j = 1, \dots, T$. The dashed white rectangle marks column 245 of matrix \mathbf{D} , showing the values of the Kullback-Leibler divergence between the frame X_{245} (systole/diastole frame) and each frame of spectrogram \mathbf{X} , i.e., $d_{KL}(X_{245}|X_j)$ where $j = 1, \dots, T$. As shown, the frames S1/S2 show a high degree of dissimilarity compared to those ones located within the intervals systole/diastole and vice versa.

169 2.1.3. Step III: Frame-level spectral divergence

170 We assume that the temporal localization of the frames S1/S2 could be based on the fact that sounds
 171 S1/S2 are shorter compared to sounds active within systole/diastole [15]. Therefore, most of the time the
 172 input PCG signal $x[m]$ is composed of the states systole/diastole with a smaller proportion of intervals
 173 S1/S2. As can be seen in Figure 5A, the dissimilarity matrix \mathbf{D} can model the frames S1/S2 by means of
 174 lobes with high temporal width, because these lobes represent the dissimilarity regarding to long intervals
 175 such as systole or diastole (see Figure 5B). However, the dissimilarity matrix \mathbf{D} models the frames associated
 176 to systole or diastole as lobes with a very low temporal width because these lobes represent the dissimilarity
 177 regarding to short intervals such as S1 or S2 (see Figure 5C). As a consequence, we propose to calculate
 178 the frame-level spectral divergence α_i , that is, the sum of the spectral divergences associated with each
 179 i^{th} frame with respect to all other frames of the matrix \mathbf{D} since this technique provides a discriminative
 180 measure to classify S1/S2 and systole/diastole frames. In other words, each value α_i , approximated by the
 181 integration over an interval by decomposing the area into trapezoids with more easily computable areas
 182 [58], represents the total area α_i under the curve defined by the dissimilarity lobes from each row i^{th}
 183 of the dissimilarity matrix \mathbf{D} . Figure 6 shows the frame-level spectral divergence α_i from the dissimilarity
 184 matrix \mathbf{D} , clearly discriminating between frames S1/S2 and frames systole/diastole. Finally, a standard
 185 peak detector is applied on the vector α to obtain the frames λ_k , $k = [1, \dots, K]$, where K is the number of
 186 sounds S1/S2 estimated. These frames λ_k are those ones with the highest frame-level spectral divergence,
 187 so they are labelled as frames S1/S2 because heart sounds S1 or S2 are active within them.

188 The pseudo-code for Stage I to roughly estimate the frames S1/S2 λ_k (at the frame level) by combining
 189 the dissimilarity matrix \mathbf{D} with the frame-level spectral divergence α_i is detailed in Algorithm 1.

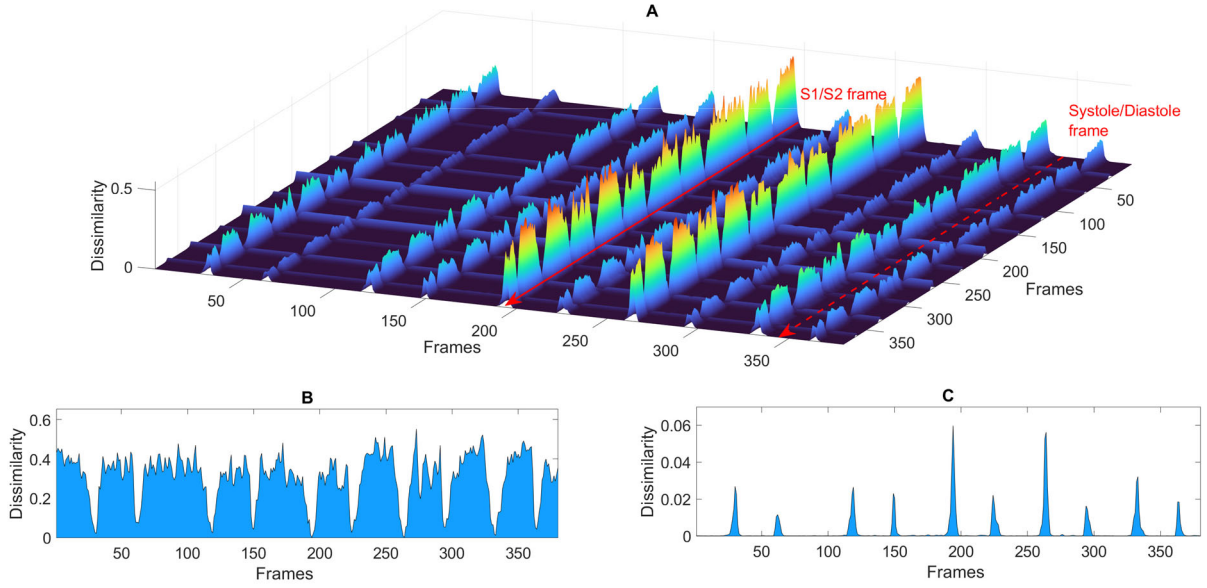


Figure 5: Example of recording "173_1307973611151 C.wav" obtained from database PASCAL [19]. A) 3D representation of the dissimilarity matrix \mathbf{D} . B) 2D representation of the area a_{192} belonging to the frame S1/S2 obtained from \mathbf{D} (solid red arrow). C) 2D representation of the area a_{347} of a frame systole/diastole obtained from \mathbf{D} (dashed red arrow).

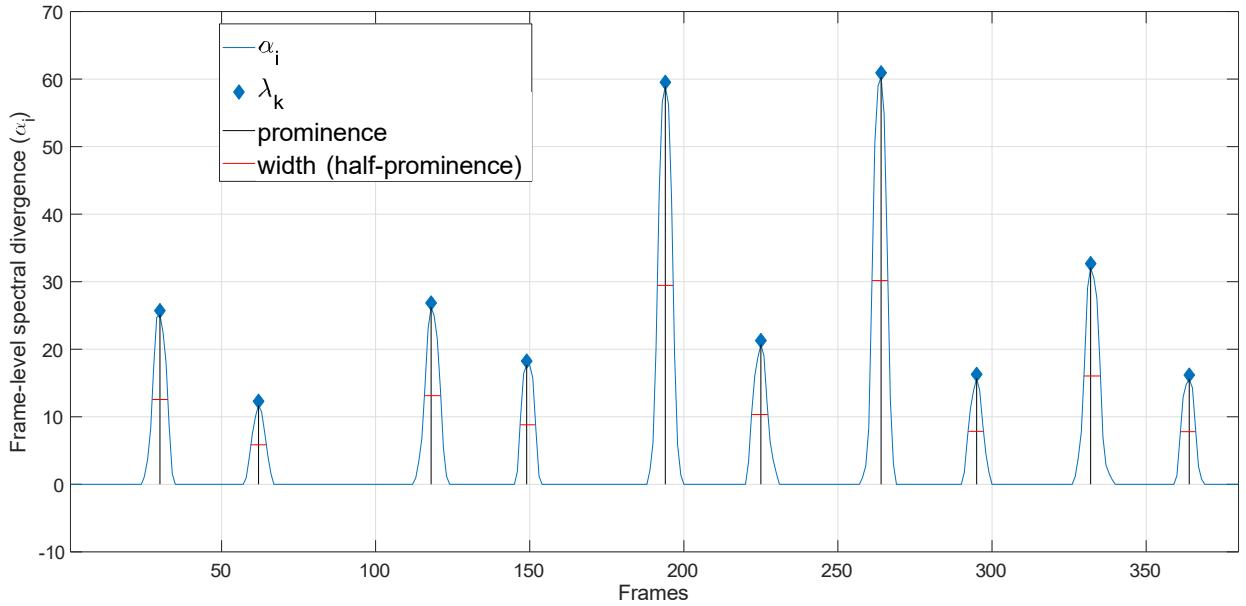


Figure 6: Example of recording "173_1307973611151 C.wav" obtained from database PASCAL [19]. The frame-level spectral divergence α_i for each row (frame) $i = 1, \dots, T$ of matrix \mathbf{D} , obtaining the detection of heart sounds S1 and S2 at frame level λ_k .

190 2.2. Stage II. Fine heartbeat detection

191 The objective of this stage is to refine the temporal localization of the frames S1/S2 λ_k obtained in
 192 Stage I, and subsequently classify them as S1 or S2. As previously mentioned, we assume that the temporal
 193 duration of cardiac systole tends to be constant over time compared to diastole intervals, so HR changes
 194 mostly due to the temporal variation of the cardiac diastole over time. Based on this, we propose a method

Algorithm 1 Rough heartbeat detection

Require: $x[m]$, N and S .

Step I: Preprocessing

1: Compute the magnitude PCG spectrogram \mathbf{X} by means of the STFT using a Hamming windows of N samples with S overlap.

2: Compute the normalised spectrogram $\bar{\mathbf{X}}$ using Equation (1).

3: Apply a band-pass filter with cut-off frequencies from 20 to 200 Hz.

Step II: Dissimilarity matrix

4: Calculate the dissimilarity matrix \mathbf{D} using Equation (2).

Step III: Frame-level spectral divergence

5: Calculate the frame-level spectral divergence α_i for each row i^{th} of the matrix \mathbf{D} .

6: Localization of the S1/S2 frames, denoted as λ_k , from the frame-level spectral divergence α_i .

return λ_k

195 based on a sliding window algorithm that validates and corrects the previously cardiac frames λ_k and then,
196 classifies them as S1 or S2. Specifically, this stage is divided into two steps which are detailed below.

197 *2.2.1. Step I: Systole duration identification*

198 The cardiac frames λ_k are converted to cardiac samples δ_k in order to improve the accuracy of the events
199 S1/S2 detected in the previous stage. For this purpose, we propose to use a window of size N along the
200 input PCG signal $x[m]$ to locate the sample δ_k associated to each frame λ_k . To do that, we select the set of
201 samples ρ_k belonging to the cardiac frame λ_k as follows,

$$\rho_k = [\lfloor \lambda_k \cdot S \cdot N \rfloor + 1, \dots, \lfloor \lambda_k \cdot S \cdot N \rfloor + N] \quad (3)$$

202 where $\lfloor \cdot \rfloor$ denotes the rounding operator to the nearest integer value to zero. Next, we determine that
203 a sound S1/S2 appears by looking for the sample δ_k with the largest amplitude within the set of samples
204 ρ_k . The procedure how the sample δ_k is computed can be observed in Figure 7.

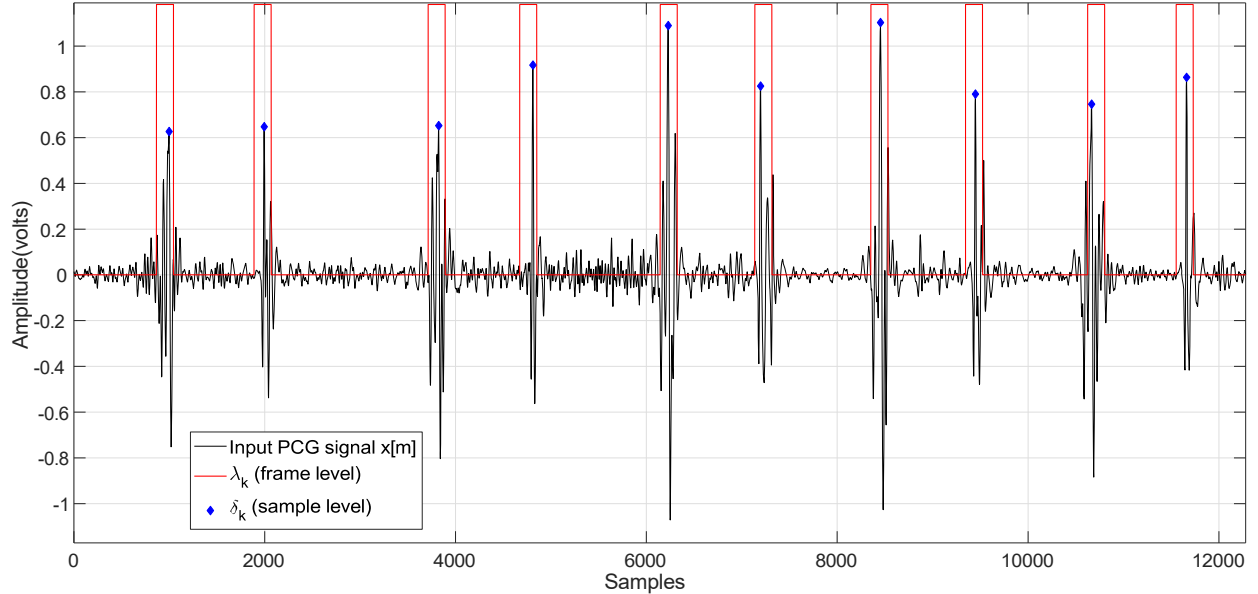


Figure 7: Example of recording "173_1307973611151_C.wav" obtained from database PASCAL [19]. Frame-level and sample-level heartbeat detection. Note that each red rectangle indicates the set of samples ρ_k , e.g., the first rectangle is composed of the samples associated to ρ_1 , the second rectangle is composed of the samples associated to ρ_2 , etc.

205 Once the heartbeat detection to a sample-level is performed, the main contribution of this step is the
 206 temporal estimation β , in samples, of the cardiac systole. In this respect, the temporal distance ζ_d , in
 207 samples, between the previous heartbeat pairs δ_k is computed as follows,

$$\zeta_d = \delta_{k+1} - \delta_k \quad \forall d, k \in [1, K - 1] \quad (4)$$

208 where ζ_d should contain the distances of the systole and diastole consecutively. Therefore, if the odd
 209 distances correspond to the systole, the even distances correspond to the diastole and vice versa (see Figure
 210 8A). Assuming that systole intervals tend to maintain a constant duration over time compared to diastole
 211 intervals as previously mentioned, we estimate the cardiac systole duration β , in samples, by extracting the
 212 most repeated distance from ζ_d . As can be seen in Figure 8B, the temporal duration of systole β is obtained
 213 by applying a histogram, composed of H bars, over the vector ζ_d . Specifically, β is equal to the center value
 214 related to the range of the bar with the highest number of repetitions. Experimental results showed that
 215 the detection performance remains stable when $H \in [5, 50]$.

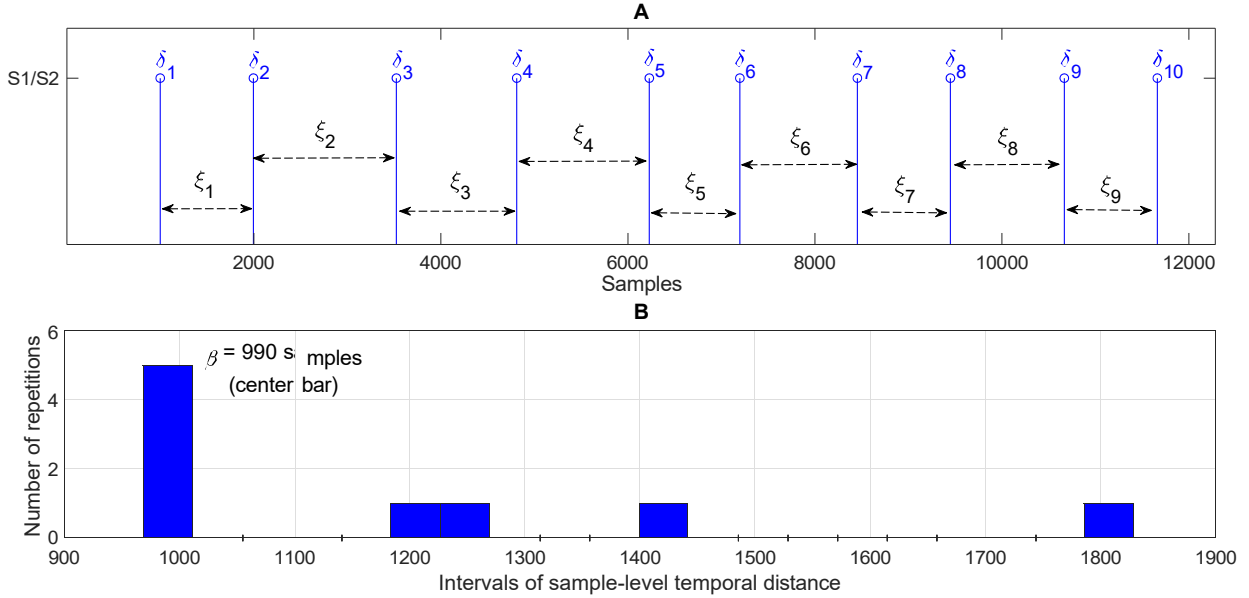


Figure 8: Example of recording "173_1307973611151_C.wav" obtained from database PASCAL [19]. A) Representation of the heartbeats S1/S2 (in a sample-level) by means of δ_k and the distances ξ_d between the previous heartbeats. B) Histogram of the distance vector ξ_d , composed of 20 bars, and the estimation of the systole interval duration β .

216 2.2.2. Step II: Heart rate estimation and S1/S2 classification

217 In order to provide an accurate description of the heartbeats S1/S2, we propose determining the initial
 218 heart rate HR_i , defined by the two most likely consecutive cardiac cycles assuming the constant temporal
 219 duration of systole β previously computed, as follows: i) the beat-to-beat distances ζ_d most likely to be
 220 systoles are estimated by means of ϕ_s , $s = 1, \dots, (K - 1)/2$, being ϕ_s the half of the distances closest to the
 221 value β ; ii) the vector ϕ_s is sorted in ascending order $\phi_s^{(sorted)}$, that is, a smaller difference between ζ_d and
 222 β means a higher probability of being a true systole; and iii) a simple search algorithm is applied to locate
 223 two systole intervals from the vector $\phi_s^{(sorted)}$ that fulfil the condition that both systole intervals have to be
 224 located consecutively within the vector ζ_d and separated by a diastole interval (that is, a distance ζ_d not
 225 contained in the vector $\phi_s^{(sorted)}$). Specifically, the algorithm starts with the most probable systole $\phi_s^{(sorted)}$
 226 and checks if any of the systoles contained in $\phi_s^{(sorted)}$ satisfy the previous condition in ζ_d . In this sense, the
 227 algorithm scans the vector $\phi_s^{(sorted)}$ until it finds two systole intervals that fulfil the previous one. Once the

228 two consecutive systole intervals $C1, C2$ are located by means of their initial positions $\delta_{S1}^{C1}, \delta_{S1}^{C2}$ and final
 229 positions $\delta_{S2}^{C1}, \delta_{S2}^{C2}$. implicitly, the localization of the associated cardiac cycles is also defined by the states
 230 S1, systole, S2 and diastole. Moreover, the initial heart rate HR_i associated to these previous consecutive
 231 cardiac cycles can be estimated either as the difference between the initial positions $|\delta_{S1}^{C2} - \delta_{S1}^{C1}|$ or final
 232 positions $|\delta_{S2}^{C2} - \delta_{S2}^{C1}|$ because the systole duration is the same for both, as shown in Figure 9.

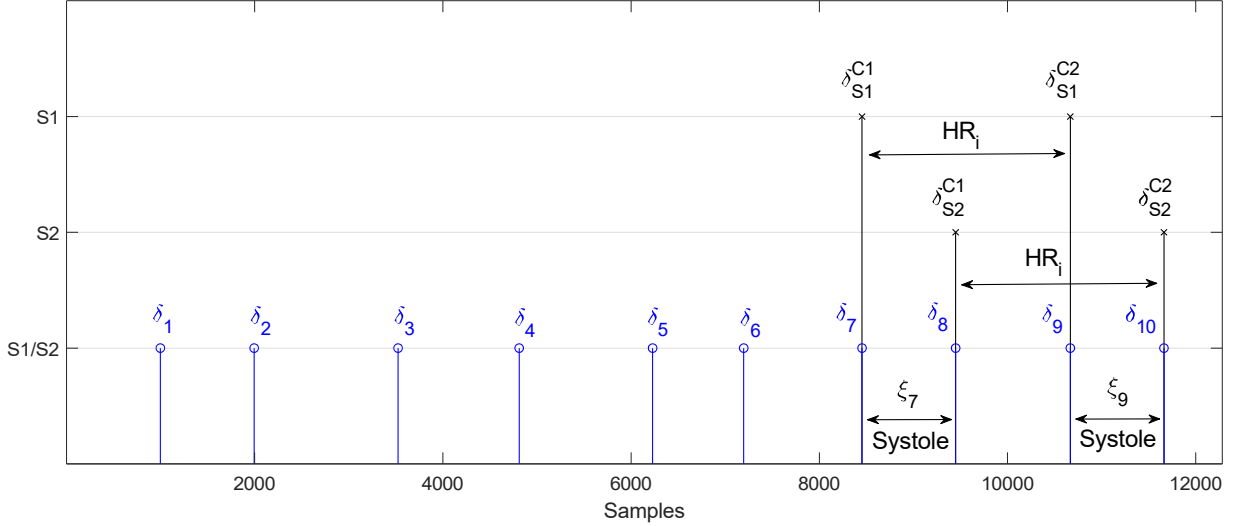


Figure 9: Example of recording "173_1307973611151_C.wav" obtained from database PASCAL [19]. Estimation process of the most likely consecutive systole intervals $C1, C2$ based on the constant systole time β . Note that once both systole intervals have been determined (ξ_7 and ξ_9), their corresponding heartbeats (S1 and S2) are implicitly labeled. The following information can be extracted at the sample-level: (i) The beginning of the systole intervals: δ_{S1}^{C1} and δ_{S1}^{C2} ; (ii) The final of the systole intervals: δ_{S2}^{C1} and δ_{S2}^{C2} ; (iii) Localization of the four states regarding a cardiac cycle: S1, systole, S2 and diastole and implicitly, the heart rate $HR_i = |\delta_{S1}^{C2} - \delta_{S1}^{C1}| = |\delta_{S2}^{C2} - \delta_{S2}^{C1}|$

233 Next, a verification-correction algorithm is proposed based on a sliding window that runs through the
 234 rest of the previously estimated heartbeats S1/S2 located by the samples δ_k . In this manner, the definiti-
 235 tive output of the heartbeat detection is provided by means of the samples $\delta_b, b = [1, \dots, B]$, being B
 236 the number of estimated heartbeats S1/S2 after the validation-correction process has been applied. The main
 237 characteristics of the sliding window are the following:

- 238 • The window slides from the right to left, starting with the two cardiac cycles associated to the previous
 239 systole intervals $C1, C2$ that define the initial heart rate HR_i , in order to perform a verification-
 240 correction of all detected heartbeats δ_k in the remaining cardiac cycles. Specifically, the window slides
 241 to the right starting from the samples δ_{S1}^{C2} and δ_{S2}^{C2} belonging to the second estimated cardiac cycle
 242 associate to the systole interval $C2$. However, the shift to the left start from the samples δ_{S1}^{C1} and δ_{S2}^{C1}
 243 belonging to the first estimated cardiac cycle associate to the systole interval $C1$. The process of the
 244 window sliding to the left can be observed in Figure 10(A.I), 10(B.I) and 10(C.I).
- 245 • The size of the sliding window applied to a given cardiac cycle is variable because the duration of the
 246 diastole does not remain constant as previously mentioned. Considering a shift d from the most likely
 247 systole intervals $C1, C2$, this window size is determined from the value HR_d of the adjacent cardiac
 248 cycle. Specifically, the adjacent cardiac cycle to the right is considered when the window slides to
 249 the left and vice versa. Following a conservative strategy, the size of the sliding window is delimited
 250 using a tolerance margin of error η , where the lower and upper boundaries of the window range within
 251 $[HR_d + \eta, HR_d - \eta]$ from the previous systole interval as shown in Figure 10. Specifically, η always
 252 has the same value at all window shifts, being used the maximum duration of the heartbeats S1 and
 253 S2 in literature. For this reason, we have used $\eta=160$ ms similarly as occurs in [15, 16, 13].

254 The verification-correction-classification algorithm performs two tasks at each of the sliding window
255 shifts: (I) a verification-correction process applied to heartbeats S1/S2 and then, a heartbeat classification
256 between S1 and S2; and (II) Updating the heart rate HR_d at each shift. Figure 10 reports an example
257 of how the previous sliding window is applied. Subfigures 10A.I, 10B.I, and 10C.I show the verification-
258 correction-classification task, which is explained below. However, Subfigures 10A.II, 10B.II and 10C.II show
259 the updating process regarding to HR_d over successive sliding window shifts. Specifically, a non-fixed value
260 of HR_d along the shifts can be observed due to the temporal variations in diastole.

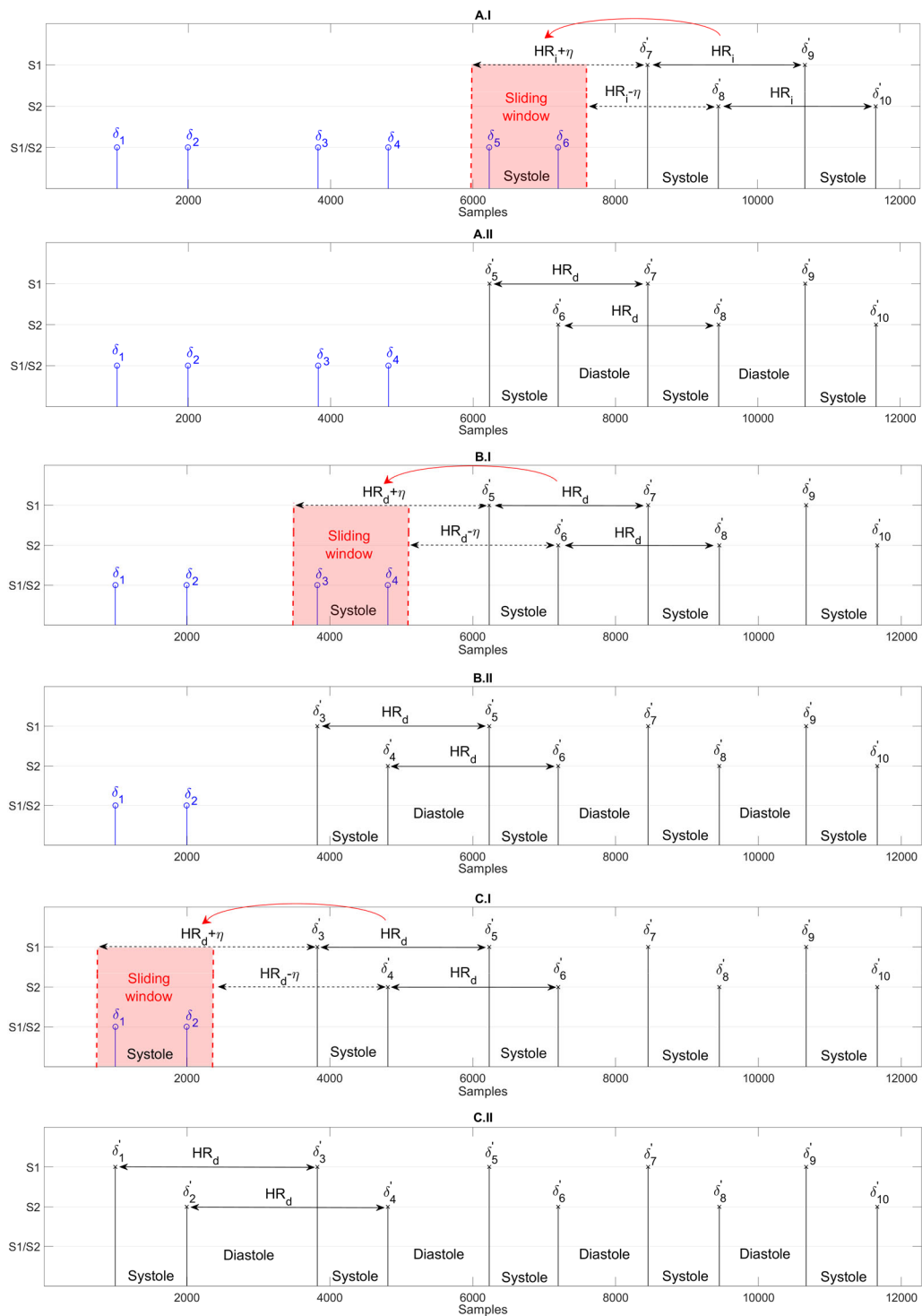


Figure 10: Example of recording "173_1307973611151_C.wav" obtained from database PASCAL [19]. The method of sliding window considering only the left shift. The subfigures show the window path composed of three shifts: A, B and C. Subfigures *.I show the verification-correction-classification task (from heartbeats S1/S2 to heartbeats S1 or S2). Subfigures *.II show the updating HR_d task. Note that the blue labels δ_k define the heartbeats S1/S2 before applying the sliding window process but the black labels δ'_k indicate the heartbeats S1 or S2 after the sliding window procedure has been applied.

261 In order to apply the verification-correction-classification task on the samples δ_k at each window shift, we
 262 propose to define a set of rules based on some characteristics typically shown by most of the heart sounds to
 263 improve the detection and classification of the heartbeats S1/S2: (i) only two heartbeats S1 and S2 can be
 264 active in each cardiac cycle; and (ii) the duration of systole has to remain constant over time. Considering
 265 the above characteristics, the verification-correction-classification task is defined analysing all scenarios that
 266 may occur in each cardiac cycle when it is analysed due to a sliding window shift. Next, we explain the four
 267 possible scenarios that can appear depending on the number of heartbeats S1/S2 detected in each cardiac
 268 cycle (see Figure 11):

- 269 • **Scenario A: no heartbeat has been detected.** A correction stage is applied adding the positions
 270 of two new heartbeats S1 and S2 to the vector δ'_b . Specifically, the new heartbeats S1 and S2 are
 271 located in the current window at the distance of HR_d from the beginning and final of the adjacent
 272 systole interval without applying the margin error η in order to maintain the constant systole criterion
 273 (see Figure 11A). Besides, the two new heartbeats are labelled S1 and S2 consecutively due to the
 274 theoretical structure of a cardiac cycle, composed of the sequence S1, systole, S2 and diastole.
- 275 • **Scenario B: only one heartbeat has been detected.** A correction stage is applied adding the
 276 position of the missing heartbeat to the vector δ_b . To determine whether the missing heartbeat is S1
 277 or S2, the lower or upper boundary of the window closest to the detected heartbeat δ_k is identified.
 278 For this purpose, the distance of the detected heartbeat δ_k from the lower boundary d_L and from the
 279 upper boundary d_U is obtained. As a consequence, two different situations appear: (i) if the detected
 280 heartbeat δ_k is closer to the lower boundary $d_L < d_U$ (see Figure 11B), the heartbeat is denoted as
 281 S1 and the new heartbeat S2, added to the vector δ'_b , is located $+\beta$ samples (systole time) of distance
 282 from S1; or (ii) if the detected heartbeat δ_k is closer to the upper boundary $d_L > d_U$, the heartbeat is
 283 denoted as S2 and the new heartbeat S1, added to the vector δ'_b , is located $-\beta$ samples (systole time)
 284 of distance from S2;
- 285 • **Scenario C: two heartbeats have been detected.** A verification stage is applied to the two
 286 detected heartbeats in the vector δ_k and a result, they are classified as S1 and S2 consecutively (see
 287 Figure 11C). Highlight that all shifts shown in Figure 10 belong to Scenario C.
- 288 • **Scenario D: more than two heartbeats have been detected.** A correction stage is applied to
 289 remove the erroneous heartbeats in the vector δ_k . For this purpose, all possible distances between all
 290 possible pairs of detected heartbeats δ_k in the current cardiac cycle are computed and those whose
 291 difference is closest to the systole time β is selected, adding the pair of values δ_k used in the closest
 292 difference to the vector δ'_b , being classified as S1 and S2 consecutively (see Figure 11D).

293 Summarizing, the output of the verification-correction-classification algorithm provides a more reliable
 294 heartbeats detection because it solves small errors that may have occurred in Stage I. Moreover, a heartbeats
 295 classification discriminating S1 and S2 is achieved, assuming the constant systole duration criterion.

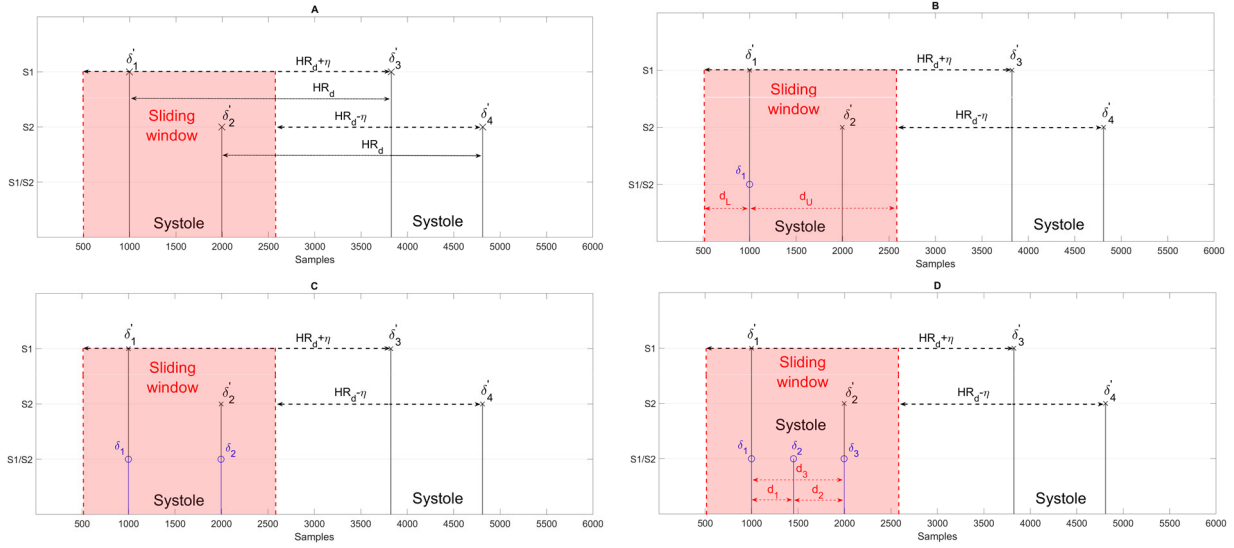


Figure 11: The four scenarios that can be found in the verification-correction-classification task when a sliding window shift is applied. A) Scenario A: no heartbeat has been detected, B) Scenario B: only one heartbeat has been detected, in this example, the heartbeat S1 by means of δ_1 . C) Scenario C: two heartbeats have been detected, in this example, the heartbeats S1 and S2 by means of δ_1 and δ_2 . D) Scenario D: more than two heartbeats have been detected, being only two of them correct. In this case, the heartbeats by means of δ_1 , δ_2 , δ_3 .

296 The pseudo-code for Stage II that allows to obtain an improved detection of heartbeats, at the sample
 297 level, and heart sound classification between S1 and S2 is shown in Algorithm 2.

Algorithm 2 Fine heartbeat detection

Require: $x[m]$, N , S and λ_k .

Step I: Systole duration identification

- 1: Localization of the samples S1/S2 by means of δ_k .
- 2: Compute the temporal distance ζ_d using Equation (4).
- 3: Compute the cardiac systole duration β .

Step II: Heart rate estimation and S1/S2 classification

- 4: Compute the two most likely consecutive systole intervals C_1 , C_2 .
- 5: Compute the initial positions $\delta_{S_1}^{C_1}$ and $\delta_{S_1}^{C_2}$ regarding to C_1 , C_2 .
- 6: Compute the final positions $\delta_{S_2}^{C_1}$ and $\delta_{S_2}^{C_2}$ regarding to C_1 , C_2 .
- 7: Compute the initial heart rate HR_i .
- 8: Compute the lower and upper boundaries $[HR_d + \eta, HR_d - \eta]$ for each window shift.
- 9: Compute δ_b applying the verification-correction-classification algorithm on the samples S1/S2 represented by means of δ_k .

return δ_b

298 **3. Evaluation**

299 *3.1. Dataset*

300 The detection/classification performance of the proposed method and other recent and relevant state-of-
 301 the-art methods has been assessed using the open access dataset PASCAL [19]. Specifically, PASCAL has
 302 been widely used in the tasks of segmentation and classification applied to PCG signals [25, 26, 7, 46, 59,
 303 16, 5, 60], since both tasks can be considered as a pre-processing stage for the detection of abnormal heart
 304 sounds. The dataset PASCAL is composed of two datasets, A and B, generated by different sources:

- Dataset A: generated from the general public via the iStethoscope Pro iPhone app. This database is composed of 176 heart sound recordings containing both normal and abnormal heart sounds. However, sample-level annotation and S1/S2 classification of heartbeats is only available for 21 of the recordings.
- Dataset B: generated from a clinic trial in several hospitals using the digital stethoscope DigiScope. This database is composed of 656 heart sound recordings, containing both normal and abnormal heart sounds. However, sample-level annotation and S1/S2 classification of heartbeats is only available for 90 of the recordings.

As a consequence, the evaluation performed in this paper has only considered those recordings that have their corresponding heartbeat annotation, resulting in a database D_T composed of 111 recordings, 21 obtained from the dataset A and the remainder 90 recordings from the dataset B.

Additionally, the database D_T has been modified by adding Additive White Gaussian noise (AWGN) with different signal-to-noise ratios (SNR) in order to evaluate the robustness of the heartbeat detection/classification algorithms. In this way, the databases $D_{T_{10}}$ (SNR = 10 dB), D_{T_5} (SNR = 5 dB), D_{T_0} (SNR = 0 dB), $D_{T_{-5}}$ (SNR = -5 dB) and $D_{T_{-10}}$ (SNR = -10 dB) refer to the previous database D_T , but using different SNR between each PCG signal $x[m]$ and the noise signal $a[m]$. For example, the database $D_{T_{10}}$ is composed of mixtures in which the power of $x[m]$ is 10 dB greater compared to $a[m]$ and so on for the rest of the databases D_{T_5} , D_{T_0} , $D_{T_{-5}}$, $D_{T_{-10}}$ taking into account their specific SNR.

To evaluate the detection/classification performance of the proposed method in a realistic sound scenario in which different kinds of clinical ambient noises are active, we have acquired a private database, denoted as D_N , through the Soundsnap¹, the world's most widely used sound effects platform. The database D_N is composed of 75 signals recorded in a real clinical environment, with duration between 45 and 307.2 seconds, in which common sounds that appear in a hospital can be heard (e.g., people talking, medical equipment noise, office equipment noise, doors opening and closing, footsteps, etc.). From the clinical noise database D_N and the PCG database D_T , the new database D_C has been created by degrading each PCG signal (database D_T) with different types of clinical noise that could be found in clinical mediums (database D_N). Specifically, the database D_C has been obtained by mixing each recording from the database D_T with a random fragment of one of the noise recordings from the database D_N .

Finally, in order to evaluate the robustness of the proposed method when PCG recordings contain abnormal heart sounds representing cardiac abnormalities, the CirCor DigiScope Phonocardiogram Dataset [61, 62] has been used. The CirCor database is composed of 5282 recordings captured from the four main auscultation locations (aortic valve, pulmonary valve, tricuspid valve and mitral valve) of 1568 subjects both with and without cardiac abnormalities. From the CirCor database, we have created the new database D_O by selecting only those PCG recordings in which abnormal heart sounds that represent different common valvular diseases (e.g., aortic stenosis, aortic regurgitation, mitral stenosis, mitral regurgitation, mitral valve prolapse, pulmonary stenosis, tricuspid stenosis, tricuspid regurgitation, septal defects and hypertrophic obstructive cardiomyopathy) are active. Specifically, the new database D_O is composed of 150 recordings with duration between 4.8 and 80.4 seconds.

3.2. Metrics

3.2.1. Heartbeat detection

Four measures [17, 16, 7], widely used in the field of biomedical signal processing, are used in order to evaluate the proposed method: *Accuracy*, *Precision*, *Recall* and *F1 – score*. All of them are calculated in a sample-by-sample level by comparing the estimated and the ground truth data. An event is considered to be correctly detected when it overlaps in sample-level with the associated event in the ground truth. Note that a maximum time shift of 80 ms in both directions of the event boundaries has been allowed, as the maximum heartbeat duration has been considered to be about 160 ms [15, 16, 13].

¹<https://www.soundsnap.com/tags/clinic>

350 Considering TP as the number of events S1/S2 correctly detected, TN as the number of events non-S1/S2
 351 correctly detected, FP as the number of events non-S1/S2 incorrectly detected and FN as the number of
 352 events S1/S2 undetected. Therefore, the four previous metrics are calculated as follows,

$$Accuracy(\%) = \left(\frac{TP + TN}{TP + TN + FP + FN} \right) \cdot 100 \quad (5)$$

$$Precision(\%) = \left(\frac{TP}{TP + FP} \right) \cdot 100 \quad (6)$$

$$Recall(\%) = \left(\frac{TP}{TP + FN} \right) \cdot 100 \quad (7)$$

$$F1 - score(\%) = \left(\frac{2TP}{2TP + FP + FN} \right) \cdot 100 \quad (8)$$

353 Specifically, *Accuracy* represents the ability to correctly detect the presence or absence of events S1/S2;
 354 *Recall* represents the ability to detect the number of missed events S1/S2 (false negatives); *Precision*
 355 represents the ability to detect the number of events S1/S2 that are inactive in the signal (false positives),
 356 and *F1 - score* indicates that both *Precision* and *Recall* are of equal importance. Note that the value of
 357 TN has not been considered in the computation of the *Accuracy* to avoid unbalancing the results, as the
 358 number of samples where the events S1/S2 are inactive is much higher than the number of samples where
 359 the events S1/S2 are active.

360 Finally, the same metric proposed in [19] has been applied to evaluate the average error associated
 361 to the heartbeats localization. Specifically, the metric labelled Total Error (TE) is computed by finding
 362 the difference, in milliseconds (ms), of the locations between the estimated one and their corresponding
 363 annotated heart sounds,

$$TE_k(ms) = \frac{\sum_{i=1}^{N_k} (RHS_i - THS_i)}{N_k} \cdot 10^3 \quad (9)$$

364 where TE_k represents the previous average error associated to the k^{th} PCG recording in the dataset;
 365 RHS_i and THS_i is the i^{th} ground truth and detected heartbeat location S1/S2 of the k^{th} PCG recording
 366 respectively; N_k is the total number of heartbeats active in the k^{th} PCG recording and f_s is the sampling
 367 frequency of the signal. For example, $TE_4 = 20ms$ indicates that the average error for the heartbeats
 368 detected in the recording number 4 is 20 ms.

369 3.2.2. Heartbeat classification

370 In order to classify an event S1/S2 between S1 or S2, the metrics proposed in [7] have been used: (1)
 371 *Accuracy*, which provides the rate of correct classification of both S1 and S2 events; (2) *Sensitivity*, which
 372 reports the correct classification of S2 events, that is, the sensitivity is referred as accuracy of class S2; and
 373 (3) *Specificity*, which provides the correct classification of S1 events, that is, the specificity is referred as
 374 accuracy of class S1.

$$Accuracy(\%) = \left(\frac{TS1 + TS2}{TS1 + TS2 + FS1 + FS2} \right) \cdot 100 \quad (10)$$

$$Sensitivity(\%) = \left(\frac{TS2}{TS2 + FS2} \right) \cdot 100 \quad (11)$$

$$Specificity(\%) = \left(\frac{TS1}{TS1 + FS1} \right) \cdot 100 \quad (12)$$

377 where $TS1$ is the number of events S1 correctly labelled as S1; $TS2$ is the number of events S2 correctly
 378 labelled as S2; $FS1$ is the number of events S1 incorrectly labelled as S2; and $FS2$ is the number of events
 379 S2 incorrectly labelled as S1.

380 3.3. Setup

381 Preliminary results showed the optimal initialisation of parameters in order to obtain the best trade-off
382 between heart sound detection/classification performance and computational cost: sampling rate $f_s = 4096$
383 Hz, Hamming window with $N = 128$ samples length and 25% overlap (temporal resolution of 7.8 ms), a
384 discrete Fourier transform using $2N$ points (frequency resolution of 16 Hz).

385 3.4. State-of-the-art methods for comparison

386 Two recent state-of-the-art detection/classification heartbeat methods have been used to evaluate the
387 performance of the proposed method: DAS [25] and MUS [26]. Both state-of-the-art methods have been
388 implemented strictly following the modules, stages, block diagram and methodology proposed in their re-
389 spective manuscripts.

390 3.5. Results

391 In this section, we assess the potential of the proposed method applied to the heartbeats detection and
392 classification from PCG signals.

393 3.5.1. Heartbeat detection

394 The performance of the proposed method and the other state-of-the-art methods in heartbeat detection is
395 evaluated. Focusing on the proposed method, this section also evaluates the heartbeat detection performance
396 provided by the output of Stage I, denoted PM I, and by the output of Stage II, denoted PM II in order to
397 measure the improvement introduced by cascading stages I and II.

398 Figure 12 shows the detection results evaluating the database D_T when PM I, PM II and the afore-
399 mentioned baseline methods DAS and MUS are performed. It reports that both PM I and PM II provide
400 the best overall detection results, for each metric, compared to the other evaluated methods. Focusing on
401 the average results obtained by PM I: i) its *Accuracy* improvement is about 11.56% (vs DAS) and 4.12%
402 (vs MUS). It suggests that PM I is more reliable in correctly detecting the presence or absence of cardiac
403 events S1/S2; ii) its *Precision* improvement is about 9.38% (vs DAS) and 1.82% (vs MUS). Thus, results
404 reveal that PM I offers a more robust detection by reducing the number of false positives, that is, events
405 non-S1/S2 incorrectly detected; iii) its *Recall* improvement is about 3.32% (vs DAS) and 3.63% (vs MUS).
406 Therefore, PM I has a more reliable detection by minimising the number of false negatives, that is, events
407 S1/S2 undetected; iv) its *F1-score* improvement is about 7.17% (vs DAS) and 2.73% (vs MUS). It can be
408 observed that PM I provides the best balance between false positives and false negatives compared to DAS
409 and MUS. As a consequence, results confirm that the heart temporal structures modelled by the dissimilar-
410 ity matrix combined with the frame-level spectral divergence (see Section 2.1) is a suitable approach to be
411 applied in heart detection since cardiac sounds show repetitive patterns along time as previously mentioned.
412 Comparing methods DAS and MUS, DAS tends to lose a smaller number of true heartbeats S1/S2 at the
413 expense of increasing the number of false alarms. However, MUS avoids to detect a higher number of false
414 positives related to heartbeats S1/S2 at the expense of losing a higher number of true heartbeats S1/S2.

415 Figure 12 shows that the best detection performance for all metrics is obtained by PM II. Specifically,
416 PM II achieves a significant improvement of approximately 2.73% (*Accuracy*), 2.03% (*Precision*), 0.81%
417 (*Recall*) and 1.45% (*F1-score*) compared to PM I, demonstrating that the verification-correction algorithm
418 used in Stage II of the proposed method (see Section 2.2) improves the heart detection performance by
419 decreasing both the number of false positives and negatives generated in the Stage I of the proposal. A
420 remarkable strength shown by PM II is that it is the only method that offers a detection performance
421 above 90% for each PCG signal evaluated in the database D_T , regardless of the detection metric analysed.
422 Additional results shown in Table 1 have been computed in order to perform a more exhaustive analysis
423 regarding the improvement achieved by PM II with respect to PM I, measuring the activation rate of the
424 Scenarios used in the verification-correction-classification algorithm by PM II evaluating the database D_T :
425 i) the highest activation rate, 85.85%, is obtained by Scenario C indicating that both heartbeats S1/S2 have
426 been detected by PM I so, PM II only classifies them. In this case, the detection improvement is less than
427 3% regardless of the metric analysed; ii) the second highest activation rate, 9.05%, corresponds to Scenario

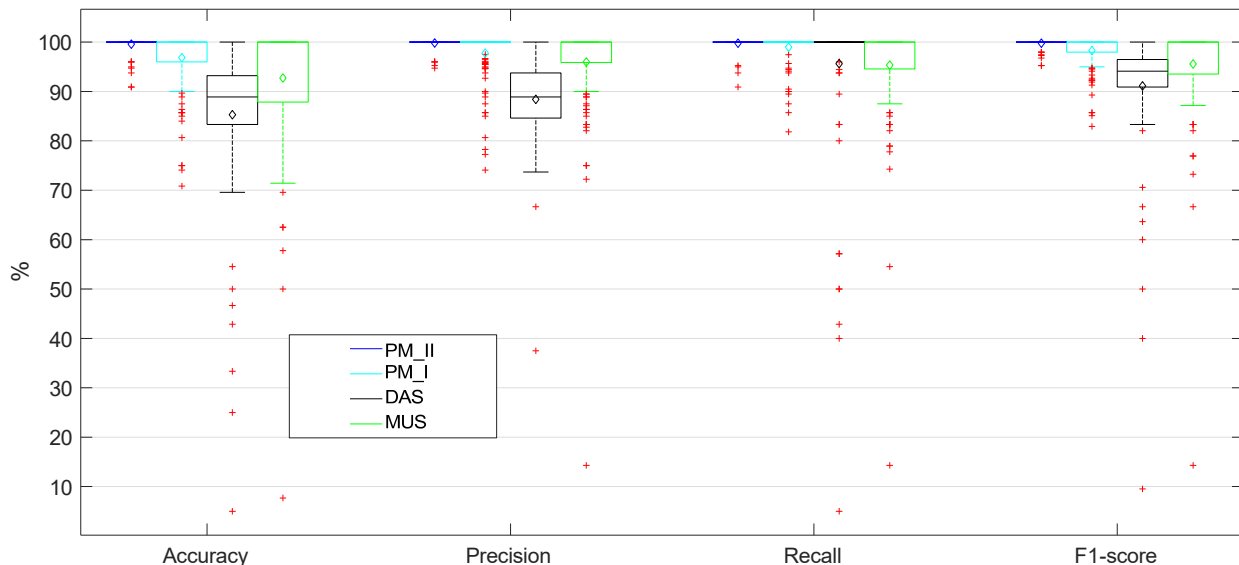


Figure 12: Heartbeats detection results, in term of *Accuracy*, *Precision*, *Recall* and *F1 - score*, evaluating the database D_T . Each box represents 111 data points, one for each PCG signal of the database D_T . The lower and upper lines of each box show the 25th and 75th percentiles. The line in the middle of each box represents the median value. The diamond shape in the center of each box represents the average value. The lines extending above and below each box show the extent of the rest of the samples, excluding outliers. Finally, outliers are defined as points that are over 1.5 times the interquartile range from the sample median, which are depicted as crosses.

428 D reporting that more than two heartbeats S1/S2 in the cardiac cycle have been previously detected by
 429 PM I. Specifically, this scenario helps to decrease the number of false positives eliminating those heartbeats
 430 erroneously detected by PM I. In this case, the detection improvement is approximately 2.03% in terms of
 431 *Precision*; iii) the third highest activation rate, 5.09%, corresponds to Scenario B in which one heartbeat,
 432 without knowing to which type S1 or S2 it belongs, of the cardiac cycle has been previously detected by
 433 PM I. This scenario allows to decrease the number of missed heartbeats S1/S2 by adding the temporal
 434 location of the heartbeats missed by PM I. The detection improvement is about 0.81% in terms of *Recall*;
 435 iv) the lowest activation rate, 0.009%, corresponds to Scenario A, where no heartbeats S1/S2 have been
 436 previously detected by PM I. This scenario has only been activated in two cardiac cycles of all PCG signals
 437 that compose the database D_T . This fact suggests that the probability of finding cardiac cycles without
 438 heartbeats detected by PM I is marginal, which confirms the efficiency in heartbeat detection provided by
 439 PM I itself.

Scenario	A	B	C	D
Activation rate	0.009%	5.091%	85.850%	9.050%

Table 1: Activation rate of the Scenarios (A, B, C and D) of the verification-correction algorithm of Stage II, belonging to the proposed method PM II evaluating the database D_T .

440 Figure 13 shows the average total error (TE) obtained for each method when the database D_T is evalu-
 441 ated. Results show that the proposed method obtains the lowest TE with a value of less than 10ms per each
 442 detected heartbeat, resulting in an improvement of 28ms compared to DAS and 63ms compared to MUS.

443 Having demonstrated that the proposed method PM II outperforms the heart detection performance
 444 compared to PM I, PM II is hereinafter referred to as the proposed method PM.

445 Figure 14 shows the detection results evaluating the database D_O in which a realistic scenario of PCG
 446 signals affected by cardiac abnormalities has been used. The results indicate that the presence of such car-
 447 diac abnormalities worsen the detection performance of all evaluated methods as it hinders the identification

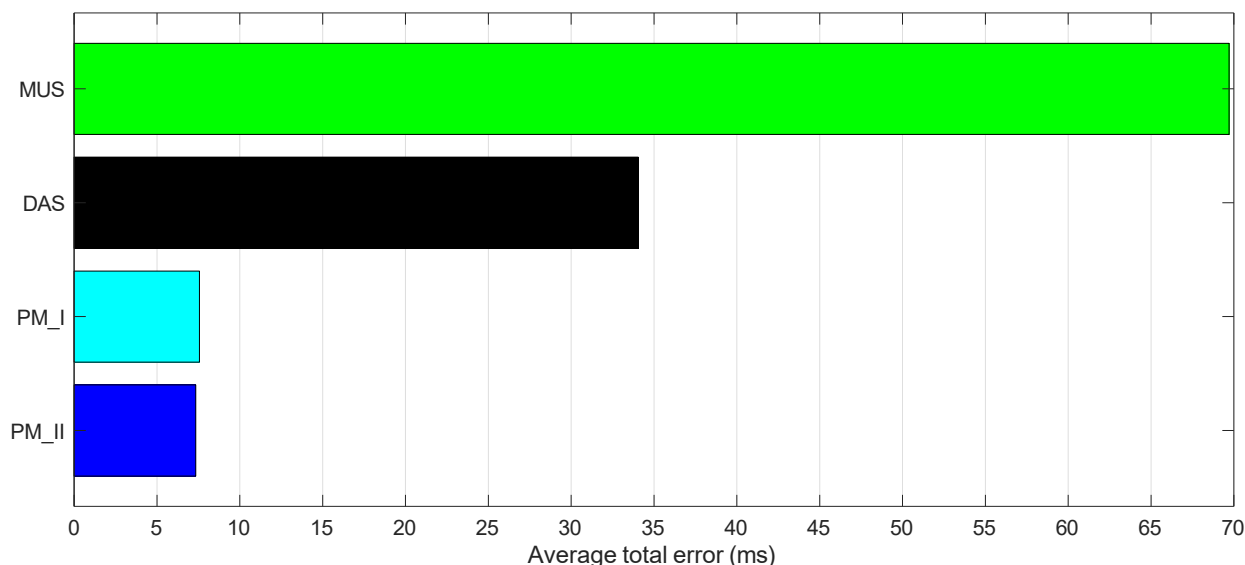


Figure 13: Average total error results, in ms, applied to heartbeat detection evaluating the database D_T .

448 of heartbeats. Thus, a drop in the average Accuracy value of 9% can be observed for the proposed method,
 449 7% for DAS and 9% for MUS. Specifically, this reduction in detection performance is associated with a
 450 remarkable dispersion in Accuracy for all evaluated methods. While the presence of anomalous heart sounds
 451 results in a higher detection of inactive S1/S2 cardiac events (false positives) provided by both the proposed
 452 method and DAS, in the MUS method there is a higher detection of inactive S1/S2 events together with a
 453 higher loss of active S1/S2 events (false negatives). The results seem to suggest that this worsening of de-
 454 tection performance is due to the fact that part of the energy of the abnormal heart sounds is located in the
 455 frequency band of heartbeats S1/S2 which makes more accurate detection difficult since some of these ab-
 456 normal sounds present high spectral similarity to normal sounds S1/S2. Nevertheless, the proposed method
 457 still provides a significant improvement over the DAS and MUS methods indicating that the temporal infor-
 458 mation provided by the dissimilarity matrix together with the proposed verification-correction-classification
 459 algorithm is still more accurate and robust than the compared approaches in correctly identifying a more
 460 or less repetitive structure that keeps appearing over cardiac cycles in which abnormal heart sounds also
 461 appear.

462 3.5.2. Heartbeat classification

463 Figure 15 shows the heartbeat classification results obtained when the database D_T is assessed comparing
 464 the performance by the proposed method PM and the aforementioned baseline methods DAS and MUS.
 465 Results report that PM provides the best overall classification scores compared to the other evaluated
 466 methods considering all classification metrics. Specifically, the proposed method achieves a remarkable
 467 improvement of approximately 30.05% (vs DAS) and 23.14% (vs MUS) in terms of average *Accuracy*.
 468 Moreover, PM accomplishes a significant improvement of approximately 32.38% (vs DAS) and 25.46% (vs
 469 MUS) in terms of average *Specificity* and 29.05% (vs DAS) and 22.09% (vs MUS) in terms of average
 470 *Sensitivity*. Although the average performance of the DAS method is worse than that achieved by MUS, it
 471 can be observed that both methods minimise both *Specificity* and *Sensitivity* in making errors in classifying
 472 both types of heartbeats S1 and S2, being, on average, slightly more inaccurate when classifying S1 events.

473 In order to determine the strengths and weaknesses of each method, an empirical analysis was also
 474 performed, extracting the following conclusions:

- 475 • **Focusing on PM**, its classification stage attempts to ensure the correct sequence of the states (S1,
 476 systole, S2, diastole) that compose the cardiac cycle. Specifically, the proposed verification-correction-

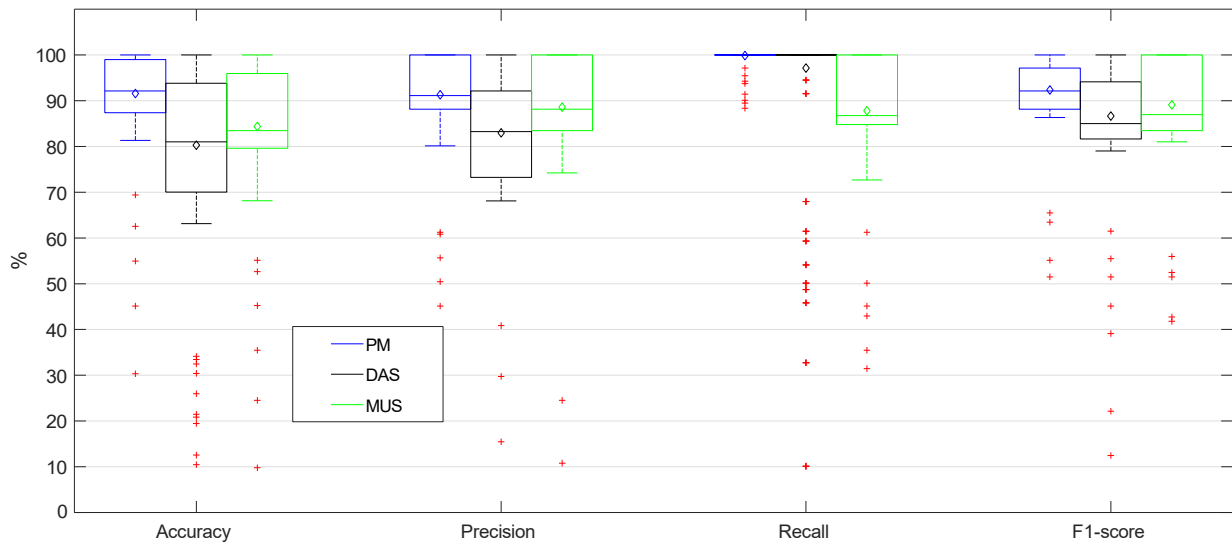


Figure 14: Heartbeats detection results, in terms of *Accuracy*, *Precision*, *Recall* and *F1 - score*, evaluating the database D_o . Each box represents 150 data points, one for each PCG signal of the database D_o . The lower and upper lines of each box show the 25th and 75th percentiles. The line in the middle of each box represents the median value. The diamond shape in the center of each box represents the average value. The lines extending above and below each box show the extent of the rest of the samples, excluding outliers. Finally, outliers are defined as points that are over 1.5 times the interquartile range from the sample median, which are depicted as crosses.

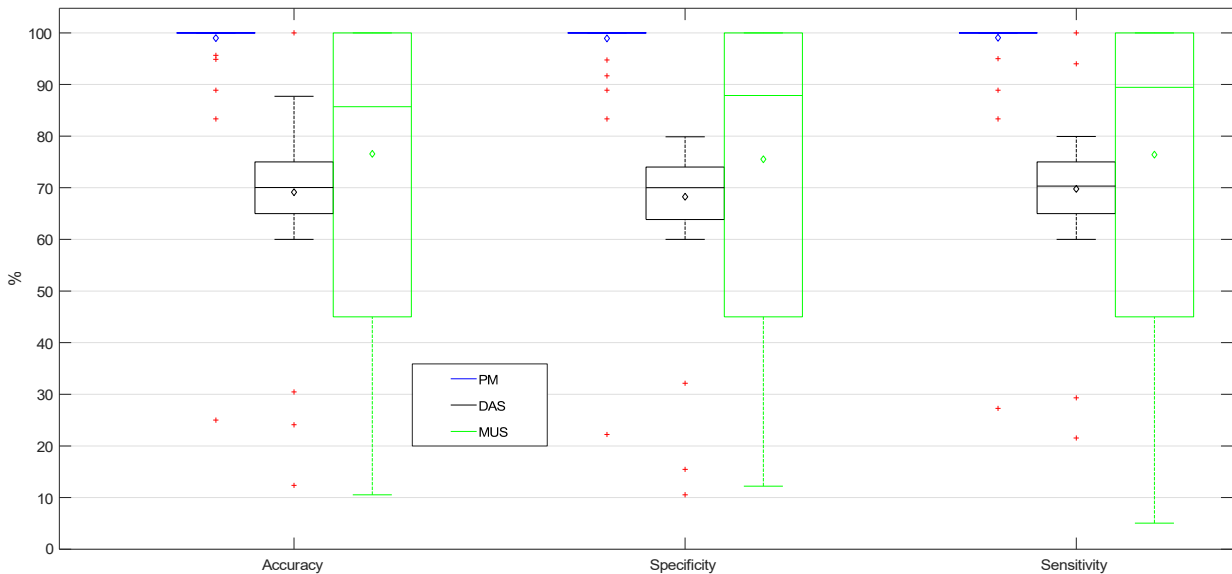


Figure 15: Heart classification results, in terms of *Accuracy*, *Specificity* and *Sensitivity*, evaluating the database D_T . Each box represents 111 data points, one for each PCG signal of the database D_T . The lower and upper lines of each box show the 25th and 75th percentiles. The line in the middle of each box represents the median value. The diamond shape in the center of each box represents the average value. The lines extending above and below each box show the extent of the rest of the samples, excluding outliers. Finally, outliers are defined as points that are over 1.5 times the interquartile range from the sample median, which are depicted as crosses.

477
478

classification algorithm based on sliding window maximises the probability that the structure of the cardiac cycles is maintained throughout the PCG signal, assuming that the duration of systole intervals

tends to be constant compared to diastole intervals, avoiding that an event FP or FN occurred in the Stage I does not interfere with the classification results. As a consequence, the classification is highly precise when the identification of the systole duration is correct (see section 2.2.1). However, the proposed method erroneously detects diastole intervals when the duration of these intervals are very similar to systole intervals. As can be seen in Figure 15, the performance obtained by the proposed method is successful since it is always above 82% for all evaluated PCG signals in the database D_T , except for only one recording, where an erroneous estimation of the systole duration was performed. Finally, the above results obtained by the proposed method are promising, since these results show a 0.89% probability of erroneously estimating the systole intervals and generating a misclassification.

- **Focusing on MUS**, the high variance, approximately 90%, shown by the results is due to its weak classification criterion. Specifically, its classification stage divides the detected heartbeats into two groups, odd and even, and labels the group with higher energy as S1 and the other as S2 [26]. In this manner, the classification results are efficient when the detection stage is correct and no FP or FN appears (in other words, if all heartbeats have been detected, then they are correctly classified). However, the performance is drastically reduced when the heartbeat detection estimates one or more than one FP or FN . For example, supposing that a given PCG signal is composed of four heartbeats S1, S2, S1 and S2, and the algorithm generates a FP detecting S1, FP , S2, S1 and S2, neither the odd elements correspond to S1 heartbeats, nor the even elements to S2 heartbeats.
- **Focusing on DAS**, the main weakness is due to its classification stage does not implement any post-processing stage to ensure the common structure of the events belonging to a cardiac cycle since it does not follow the alternation between the occurrence of two types of heartbeats S1 and S2. As a consequence, DAS allows several consecutive heartbeats to be labelled as the same type S1 or S2 [25].

Figure 16 shows the results of the classification evaluating the database D_O in which a realistic scenario of PCG signals affected by cardiac abnormalities has been used. Again, the results indicate that the presence of such cardiac abnormalities reduces the classification performance of all the methods evaluated, however, the observed reduction in the average value of Accuracy, as well as the increase in the dispersion associated with Accuracy, is greater in the classification task compared to the detection task for all methods compared. However, and as occurred when evaluating PCG signals without abnormal heart sounds, the lowest dispersion is obtained by the proposed method, followed by DAS and finally MUS, which presents the highest dispersion. Specifically, this worsening of classification performance is due, with approximately equal importance, to the errors made in the classification of the S1 and S2 events obtained by the proposed method and DAS, while the errors made by MUS mainly affect the S1 events. It should be noted that the remarkable dispersion behavior obtained by the proposed method confirms that the set of rules on which the proposed verification-correction-classification algorithm is based is capable of correctly segmenting and classifying most PCG signals, including those with presence of abnormal heart sounds, since the algorithm eliminates most of the spurious S1/S2 events and recovers the missed S1/S2 events in previous stages, guaranteeing the correct sequence of the states S1, systole, S2, diastole that compose the structure of a cardiac cycle.

3.5.3. Heartbeat detection/classification under simulated noisy conditions

Table 2 shows *Accuracy*, *Precision*, *Recall* and *F1 – score* results in order to evaluate the heartbeat detection robustness of the proposed method PM and the baseline methods DAS and MUS using five different SNR datasets: $D_{T_{10}}$, D_{T_5} , D_{T_0} , $D_{T_{-5}}$ and $D_{T_{-10}}$. Experimental results indicate that PM provides the best overall detection performance compared to the other evaluated baseline methods considering all SNR scenarios assessed. Focusing on the worst evaluated acoustic scenario $D_{T_{-10}}$ in which the AWGN noise is louder than the heart sounds, it can be observed an improvement about 14.20% (vs DAS) and 11.89% (vs MUS) in *Accuracy*, 4.93% (vs DAS) and 6.79% (vs MUS) in *Precision*, 9.62% (vs DAS) and 6.29% (vs MUS) in *Recall* and finally, 7.07% (vs DAS) and 5.56% (vs MUS) in *F1 – score*. Results confirm that PM is the most effective and reliable method for detecting heartbeats under AWGN noisy scenarios, providing a performance of over 94% for all metrics and SNR analysed. This robustness shown by PM can

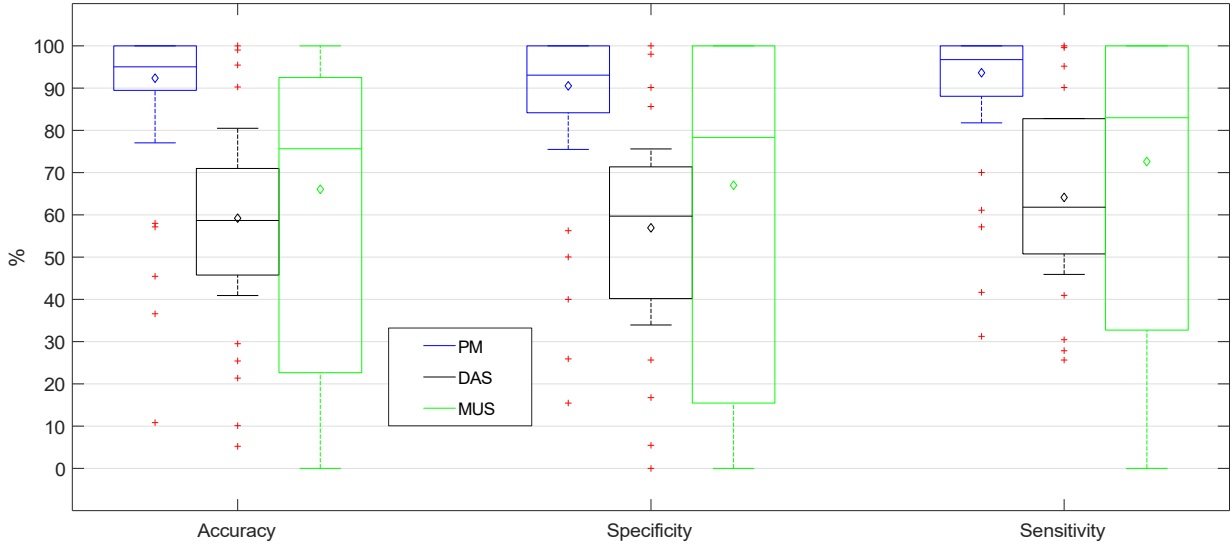


Figure 16: Heart classification results, in terms of *Accuracy*, *Specificity* and *Sensitivity*, evaluating the database D_o . Each box represents 150 data points, one for each PCG signal of the database D_o . The lower and upper lines of each box show the 25th and 75th percentiles. The line in the middle of each box represents the median value. The diamond shape in the center of each box represents the average value. The lines extending above and below each box show the extent of the rest of the samples, excluding outliers. Finally, outliers are defined as points that are over 1.5 times the interquartile range from the sample median, which are depicted as crosses.

527 be considered a promising ability to detect the presence of weak heartbeats that can be acoustically masked
 528 in noisy environments.

529 Comparing the detection results from the datasets $D_{T_{10}}$ and $D_{T_{-10}}$ that simulate the most harmful and
 530 beneficial noisy scenario, they show a performance reduction of about 4.51% (PM), 5.75% (DAS) and 9.91%
 531 (MUS) in *Accuracy*, 4.67% (PM), 8.8% (DAS) and 8.6% (MUS) in *Precision*, 1.66% (PM), 7.93% (DAS)
 532 and 3.61% (MUS) in *Recall* and 4.37% (PM), 4.63% (DAS) and 5.93% (MUS) in *F1 - score*. Note that
 533 PM suffers the smallest drop in performance compared to the other state-of-the-art methods, at best with a
 534 reduction by a factor of 4. As a result, it can be stated that the proposed method using temporal information
 535 from the dissimilarity matrix applied to the localization/classification of the heartbeats is an efficient and
 536 reliable tool, even when the PCG signal can be masked with AWGN noise that overlaps the same spectral
 537 bands at the same time of the heart sounds.

538 Table 3 shows *Accuracy*, *Specificity* and *Sensitivity* classification results, evaluating the previous five
 539 SNR datasets to compare the robustness of the S1/S2 heartbeat classification task of the proposed method
 540 and the state-of-the-art methods. The results report that PM obtains the best classification results regardless
 541 of the metric and for all the SNR scenarios evaluated. Specifically, PM is the only method that achieves
 542 that its worst performance is above 90% in all the evaluated datasets while DAS and MUS obtain results
 543 below 80% in all the SNR scenarios, even with values below 72% when $SNR < 0dB$ and implicitly, a greater
 544 time-frequency overlapping between noise and heart sounds occurs. Due to both the above results and
 545 the fact that PM reduces its performance by a smaller percentage than DAS and MUS as the SNR of the
 546 simulated scenario decreases, PM confirms its best heart classification performance in noisy environments.
 547 Thus, PM reduces its average *Accuracy* performance by approximately 7% while DAS and MUS reduce
 548 it by 9% and 11% when comparing the most harmful ($SNR = -10dB$) and beneficial ($SNR = 10dB$) acoustic
 549 environments evaluated.

550 Figure 17 and Figure 18 show the detection and classification results evaluating the database D_c in
 551 which a realistic scenario of PCG signals affected by different types of clinical environmental noise has been
 552 created. As occurs when evaluating PCG signals in which abnormal heart sounds appear, the presence of
 553 different types of ambient noises that can be found in clinical settings worsen the detection and classification

Algorithm	Accuracy (%)	Precision (%)	Recall (%)	F1 – score (%)
Database $D_{T_{10}}$ (SNR = 10dB)				
PM	99.38	99.63	99.69	99.66
DAS	86.41	89.00	96.33	91.83
MUS	92.88	96.15	95.34	95.65
Database D_{T_5} (SNR = 5dB)				
PM	99.37	99.62	99.69	99.65
DAS	85.18	88.75	95.12	91.03
MUS	92.79	95.95	95.30	95.54
Database D_{T_0} (SNR = 0dB)				
PM	99.11	99.47	99.57	99.51
DAS	84.63	88.05	93.39	90.51
MUS	92.44	95.53	95.08	95.40
Database $D_{T_{-5}}$ (SNR = -5dB)				
PM	97.16	97.61	99.12	98.09
DAS	82.27	87.56	91.26	88.97
MUS	87.54	92.92	92.41	92.50
Database $D_{T_{-10}}$ (SNR = -10dB)				
PM	94.87	94.96	98.02	95.28
DAS	80.66	85.03	88.40	87.20
MUS	82.97	88.17	91.73	89.71

Table 2: Detection results, in terms of *Accuracy*, *Precision*, *Recall* and *F1 – score*, evaluating the databases $D_{T_{10}}$, D_{T_5} , D_{T_0} , $D_{T_{-5}}$ and $D_{T_{-10}}$.

554 performance of all the methods evaluated. This reduction in detection and classification affects the proposed
555 method to a lesser extent, which continues to significantly exceed the performance shown by DAS and MUS.
556 However, in all the methods evaluated, the drop in performance in the classification task is more notable.
557 Focusing on detection, the presence of clinical ambient noise causes both the proposed method and DAS the
558 same performance when no ambient noises are active, while MUS increases the creation of spurious heart
559 events and the loss of heart events S1 and S2, which could be considered more critical for future analysis of
560 heart sound abnormalities. It is noteworthy that while DAS and MUS significantly increase the dispersion
561 of the Accuracy results in detection and classification, higher in classification (8% with respect to DAS and
562 10% with respect to MUS) compared to detection, the proposed method maintains the dispersion values
563 approximately constant with respect to the scenario without interference from ambient noise. It should be
564 noted that the high dispersion obtained by MUS is mainly due to the fact that it bases its classification
565 on a criterion based on the energy levels of heart sound events, a poor criterion when evaluating realistic
566 environments with ambient noise interference since the acoustic mixture of clinical ambient noise could
567 often cause the presence of heart events S2 with greater energy than events S1. Although DAS ranks worst
568 in terms of classification at the expense of showing lower dispersion compared to MUS, its classification
569 performance could be improved by adding a control algorithm that would allow discerning the occurrence
570 of a new heart event S1 or S2 as long as the cardiac temporal repetitive structure is maintained.

571 4. Discussion

572 In this study, we addressed the tasks of detection and classification in single-channel PCG recordings
573 using an unsupervised approach based on time–frequency behaviors shown by most of heartbeats. From a
574 medical point of view, the analysis of PCG signals allows a low-cost, non-invasive and reliable diagnosis to
575 be applied in poor-resources areas. From an engineering point of view, detection and classification using
576 signal processing in PCG signals can help the clinician to better interpret the meaning of heart sounds heard
577 through medical devices, as well as be used as a pre-processing tool to develop algorithms to identify the

Algorithm	Accuracy (%)	Specificity (%)	Sensitivity (%)
Database $D_{T_{10}}$ (SNR = 10dB)			
PM	97.18	97.12	97.24
DAS	70.29	69.01	70.76
MUS	77.59	78.24	79.66
Database D_{T_5} (SNR = 5dB)			
PM	95.53	95.47	95.59
DAS	68.49	67.79	68.38
MUS	75.00	76.99	77.00
Database D_{T_0} (SNR = 0dB)			
PM	92.68	92.62	92.74
DAS	67.47	66.88	67.46
MUS	72.33	73.54	74.55
Database $D_{T_{-5}}$ (SNR = -5dB)			
PM	91.49	91.89	91.39
DAS	64.98	64.00	65.07
MUS	70.00	71.05	71.99
Database $D_{T_{-10}}$ (SNR = -10dB)			
PM	90.79	91.10	90.51
DAS	61.41	60.90	61.00
MUS	66.78	67.49	68.64

Table 3: Classification results, in terms of *Accuracy*, *Specificity* and *Sensitivity*, evaluating the databases $D_{T_{10}}$, D_{T_5} , D_{T_0} , $D_{T_{-5}}$ and $D_{T_{-10}}$.

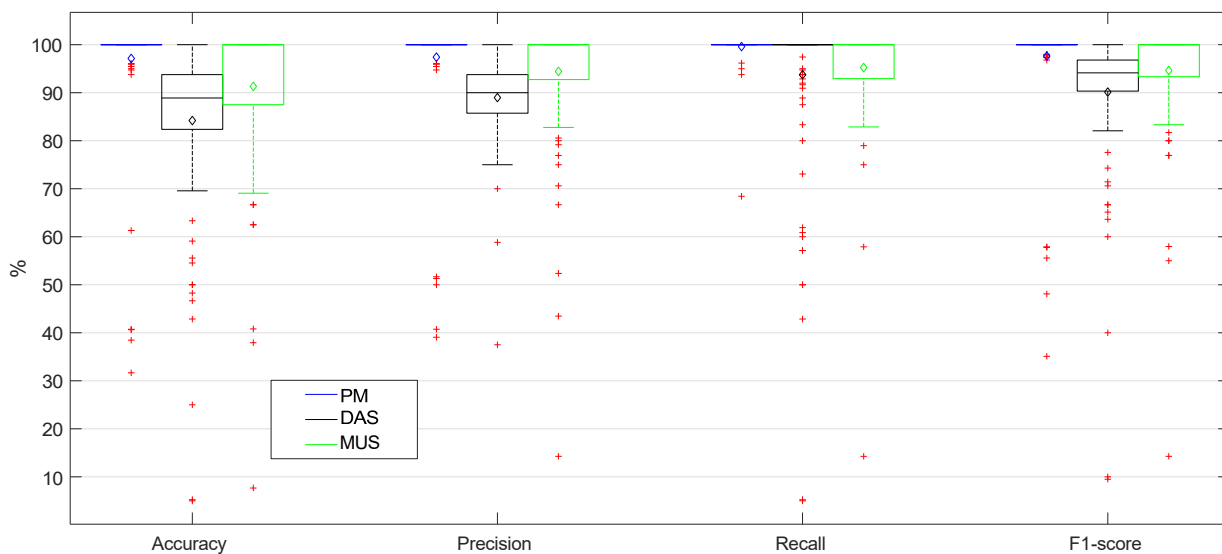


Figure 17: Heartbeats detection results, in terms of *Accuracy*, *Precision*, *Recall* and *F1 - score*, evaluating the database D_C . Each box represents 111 data points, one for each PCG signal of the database D_C . The lower and upper lines of each box show the 25th and 75th percentiles. The line in the middle of each box represents the median value. The diamond shape in the center of each box represents the average value. The lines extending above and below each box show the extent of the rest of the samples, excluding outliers. Finally, outliers are defined as points that are over 1.5 times the interquartile range from the sample median, which are depicted as crosses.

578 presence of cardiac diseases by learning the target spectral content located in specific temporal intervals
579 localized by the previous tasks.

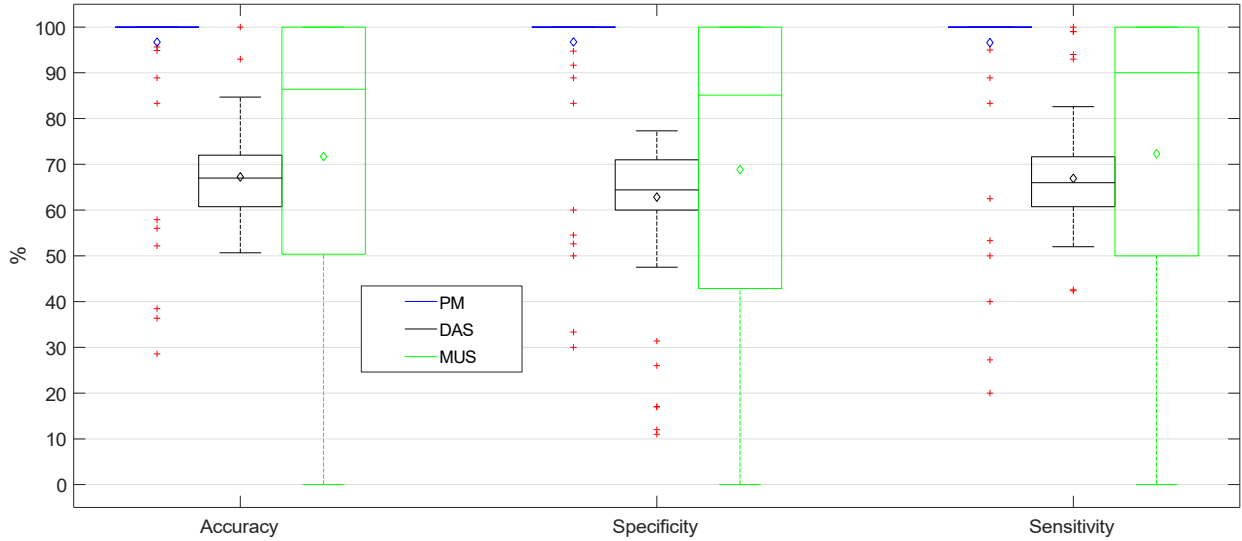


Figure 18: Heart classification results, in terms of *Accuracy*, *Specificity* and *Sensitivity*, evaluating the database D_c . Each box represents 111 data points, one for each PCG signal of the database D_c . The lower and upper lines of each box show the 25th and 75th percentiles. The line in the middle of each box represents the median value. The diamond shape in the center of each box represents the average value. The lines extending above and below each box show the extent of the rest of the samples, excluding outliers. Finally, outliers are defined as points that are over 1.5 times the interquartile range from the sample median, which are depicted as crosses.

580 The detection and classification tasks described in this study have been specially developed to analyze
581 the temporal structure exhibited by most heart sounds. Of the two cascaded stages of which the proposed
582 system is composed, the first stage attempts to detect S1 and S2 heart sounds by assuming a temporally
583 repetitive cardiac spectral structure where similar spectral patterns are observed between S1 and S2 but
584 different from the patterns that can be found in systole and diastole and, in addition, the duration of both
585 S1 and S2 is shorter than systole and diastole. For that, we propose to model such temporal structure using
586 the dissimilarity matrix that exploits the aforementioned behaviors in most heart sounds. To improve the
587 temporal localization of the heartbeats obtained in the first stage and subsequently classify them as S1 or
588 S2, the second stage presents a verification-correction-classification algorithm assuming that only two heart
589 sounds S1 and S2 can be active in each cardiac cycle and the duration of systole can be considered constant
590 over time.

591 An exhaustive assessment has been carried out, analyzing PCG signals with and without the interference
592 caused by abnormal heart sounds and different kinds of noise such as clinical ambient noise, in order to
593 evaluate both the detection and classification performance of the proposed method. Results indicated a
594 significant detection and classification improvement of the proposed method compared to the state-of-the-
595 art methods evaluated, showing that the use of the dissimilarity matrix to extract temporal information
596 from PCG signals is a promising tool to be applied in heart segmentation and further, to be applied as
597 a pre-processing stage to heart sound signal processing. While a notable strength shown by the proposed
598 method is its ability to update the heart rate by analysing a new cardiac cycle within the time structure
599 corresponding to the entire PCG signal, in addition, it is the only method evaluated that provides a detection
600 performance above 90% for each PCG signal in the database D_T . However, a weakness of the proposed
601 method is that it often erroneously detects a diastole interval when the duration of this interval is very
602 similar to the duration of a systole interval. The verification-correction-classification algorithm significantly
603 minimizes the number of false positives and false negatives initially detected because all the possible heart
604 sound scenarios, that can appear depending on the number of heartbeats detected in the first stage, can be
605 corrected.

606 Considering both the presence of abnormal heart sounds and the different types of ambient noises that

607 can be found in clinical environments, it is observed as a general behavior that all methods evaluated worsen
608 their detection and classification results. This performance reduction affects to a lesser extent the proposed
609 method, which still significantly outperforms DAS and MUS. Focusing on the acoustic interference caused
610 by the presence of clinical ambient noise, it is noteworthy that while DAS and MUS significantly increase
611 their dispersion of the Accuracy results in detection and classification, the proposed method maintains its
612 dispersion values approximately constant with respect to the scenario without interference from ambient
613 noise. As a result, our approach can be considered reliable even when the PCG signal is masked with
614 different types of noise which appear superimposed at the same time as the heart sounds as well as in the
615 same spectral band in which the heartbeats concentrate most of their energy. Focusing on the acoustic
616 interferences caused by the presence of abnormal heart sounds, it can be observed that the set of rules on
617 which the proposed verification-correction-classification algorithm is based correctly segments and classifies
618 most of the PCG signals including those with the presence of abnormal heart sounds, as the algorithm allows
619 to eliminate a large number of spurious S1/S2 events as well as to recover most of the missing S1/S2 events.
620 It can be considered another strength shown by our proposal since these facts ensure a correct, time-ordered
621 sequence of the S1, systole, S2, diastole states that make up the structure of a cardiac cycle.

622 5. Conclusions and Future work

623 In this work, we propose an unsupervised approach to detect and classify heartbeats from PCG signals.
624 In order to simulate the temporal-spectral behaviour of heart sounds, the proposed method assumes the
625 following hypotheses: i) heart sounds can be considered as spectral structures that repeat over time; ii) S1
626 and S2 heartbeats show similar spectral patterns to each other, but sufficiently different from those that can
627 be contained in the systole and diastole; iii) the duration of S1 and S2 heartbeats is always shorter than
628 systole and diastole; and iv) systole intervals tend to maintain a constant duration over time compared to
629 diastole intervals. In the detection stage, our main contribution proposes a novel version of the standard
630 similarity matrix, named dissimilarity matrix, combined with the frame-level spectral divergence in order
631 to estimate heartbeats assuming both the repetitiveness typically shown by the heart sounds and temporal
632 relationships between events S1/S2 and non-S1/S2 (systole and diastole). In the classification stage, our
633 main contribution develops a verification-correction-classification method, based on a sliding window, that
634 allows maintaining the structure of the cardiac cycle throughout the PCG signal by means of S1, systole,
635 S2 and diastole. The most relevant conclusions obtained in the experimental results are detailed below:

- 636 • The proposed method obtains the best performance in heartbeat detection, providing average results
637 above 99% and 92% for PCG signals without and with cardiac abnormalities, regardless of the met-
638 rics analysed. In this sense, the results suggest that the dissimilarity matrix is an effective tool for
639 estimating heartbeats from the PCG signal.
- 640 • The proposed method obtains the best classification performance for S1 and S2 heartbeats, offering av-
641 erage results higher than 97% and 92% for PCG signals without and with cardiac anomalies, regardless
642 of the metric analysed. In this sense, the results indicate that the algorithm based on sliding window
643 tracking to maintain the structure of the cardiac cycle is reliable to be applied in the segmentation of
644 the heartbeats of each cycle.
- 645 • Similar to what occurs in the real world, detecting and classifying heartbeats is much more com-
646 plex in acoustic scenarios in which heart sounds are barely audible due to the time-frequency overlap
647 of some kind of acoustic interference, such as AWGN noise. In this respect, highlight that the de-
648 tection/classification results of the proposed method show the smallest drop compared to the other
649 state-of-the-art methods. Specifically, comparing the evaluation of the databases $D_{T_{10}}$ and $D_{T_{-10}}$,
650 the detection results provided by the proposed method drop below 4.5% (DAS drops below 5.8% and
651 MUS 9.9%) and the classification results drop below 6.7% (DAS drops below 8.9% and MUS 10.8%),
652 in terms of *Accuracy*. It suggest that the proposed method is more robust than baseline methods in
653 the assessment of noisy scenarios, specifically, $SNR < 0dB$. Moreover, considering a realistic scenario

654 in which different kinds of clinical ambient noises are active, the proposed method obtains the best
655 heartbeat detection/classification performance, providing average results above 96% regardless of the
656 metric employed. These results indicate that the proposed method is the most robust method among
657 those evaluated when real clinical scenarios are assessed.

- 658 • Finally, the proposed method estimates the lowest temporal error compared to the other state-of-the-
659 art methods. Specifically, the proposed method produces an error of less than 10 ms per each detected
660 heartbeat, while the other methods exceed 34 ms.

661 Future work will focus in two directions: (i) normal/abnormal heart classification using heart segmenta-
662 tion provided by the proposed method that will be used as a pre-processing stage, and (ii) development of
663 novel time-frequency representations that improve the extraction of features to be applied to neural network
664 architectures in order to classify major CVDs, such as mitral stenosis and mitral regurgitation.

665 **Funding**

666 This work was supported by the Programa Operativo FEDER Andalucía 2014-2020 under project with
667 reference 1257914, the Ministry of Economy, Knowledge and University, Junta de Andalucía under Project
668 P18-RT-1994 and the Spanish Ministry of Science and Innovation under Project PID2020-119082RB-C21.

669 **Conflict of interest**

670 The authors have no conflict of interest to disclose. The authors are responsible for the content and
671 writing of this article alone.

672 **Acronyms**

AWGN	Additive White Gaussian Noise
BPM	Beats Per Minute
CNN	Convolutional Neural Network
CVD	Cardiovascular Disease
ECG	Electrocardiography
HMM	Hidden Markov Model
HR	Heart Rate
MFCC	Mel-Frequency Cepstral Coefficients
MRI	Medical Resonance Imaging
PCG	Phonocardiogram
S ₁	Heartbeat associated with the onset of systole
S ₂	Heartbeat associated with the onset of diastole
SNR	Signal-to-Noise Ratio
STFT	Short-Time Fourier Transform
SVM	Support Vector Machine
WHO	World Health Organization

674 **References**

- 675 [1] World Health Organization. Cardiovascular Diseases, [https://www.who.int/health-topics/cardiovascular-diseases/](https://www.who.int/health-topics/cardiovascular-diseases/#tab=tab_1)
676 #tab=tab_1, online. Accessed: 2021-12-20 (2022).
- 677 [2] Susanna Sans Menendez, Enfermedades Cardiovasculares, Institut d' Estudis de la Salut, Barcelona, 2021, https://www.sanidad.gob.es/organizacion/sns/planCalidadSNS/pdf/equidad/07modulo_06.pdf,
678 //www.sanidad.gob.es/organizacion/sns/planCalidadSNS/pdf/equidad/07modulo_06.pdf, online. Accessed: 2021-12-20
679 (2021).
- 680 [3] Horizon Europe Work Programme 2021-2022 4. Health, 2021, [https://ec.europa.eu/info/funding-tenders/](https://ec.europa.eu/info/funding-tenders/opportunities/docs/2021-2027/horizon/wp-call/2021-2022/wp-4-health_horizon-2021-2022_en.pdf)
681 opportunities/docs/2021-2027/horizon/wp-call/2021-2022/wp-4-health_horizon-2021-2022_en.pdf,
682 //ec.europa.eu/info/funding-tenders/opportunities/docs/2021-2027/horizon/wp-call/2021-2022/wp-4-health_horizon-2021-2022_en.pdf, online. Ac-
682 cessed: 2021-12-20 (2021).

- 683 [4] World Health Organization. Data and statistics, [https://www.euro.who.int/en/health-topics/](https://www.euro.who.int/en/health-topics/noncommunicable-diseases/cardiovascular-diseases/data-and-statistics)
684 [noncommunicable-diseases/cardiovascular-diseases/data-and-statistics](https://www.euro.who.int/en/health-topics/noncommunicable-diseases/cardiovascular-diseases/data-and-statistics), online. Accessed: 2021-12-20 (2021).
- 685 [5] P. Sharma, S. A. Imtiaz, E. Rodriguez-Villegas, An algorithm for heart rate extraction from acoustic recordings at the
686 neck, *IEEE Transactions on Biomedical Engineering* 66 (1) (2019) 246–256. doi:10.1109/TBME.2018.2836187.
- 687 [6] G. Seravalle, G. Grassi, Heart rate as cardiovascular risk factor, *Postgraduate Medicine* 132 (4) (2020) 358–367. doi:
688 10.1080/00325481.2020.1738142.
- 689 [7] Q. ul Ain Mubarak, M. U. Akram, A. Shaukat, F. Hussain, S. G. Khawaja, W. H. Butt, Analysis of pcg signals using
690 quality assessment and homomorphic filters for localization and classification of heart sounds, *Computer Methods and*
691 *Programs in Biomedicine* 164 (2018) 143–157. doi:10.1016/j.cmpb.2018.07.006.
- 692 [8] N. Giordano, M. Knaflitz, A novel method for measuring the timing of heart sound components through digital phono-
693 cardiography, *Sensors* 19 (8) (2019). doi:10.3390/s19081868.
- 694 [9] F. Renna, J. Oliveira, M. T. Coimbra, Deep convolutional neural networks for heart sound segmentation, *IEEE Journal*
695 *of Biomedical and Health Informatics* 23 (6) (2019) 2435–2445. doi:10.1109/JBHI.2019.2894222.
- 696 [10] W. Chen, Q. Sun, X. Chen, G. Xie, H. Wu, C. Xu, Deep learning methods for heart sounds classification: A systematic
697 review, *Entropy* 23 (6) (2021). doi:10.3390/e23060667.
- 698 [11] H. Liang, S. Lukkarinen, I. Hartimo, Heart sound segmentation algorithm based on heart sound envelopegram, in: *Computers*
699 *in Cardiology* 1997, 1997, pp. 105–108. doi:10.1109/CIC.1997.647841.
- 700 [12] G. Shah, P. Koch, C. B. Papadias, Analysis of acoustic cardiac signals for heart rate variability and murmur detection
701 using nonnegative matrix factorization-based hierarchical decomposition, in: 2014 IEEE International Conference on
702 Bioinformatics and Bioengineering, 2014, pp. 46–53. doi:10.1109/BIBE.2014.14.
- 703 [13] K. A. Babu, B. Ramkumar, M. S. Manikandan, Automatic identification of s1 and s2 heart sounds using simultaneous
704 pcg and ppg recordings, *IEEE Sensors Journal* 18 (22) (2018) 9430–9440. doi:10.1109/JSEN.2018.2869416.
- 705 [14] L. S. Lilly, Pathophysiology of heart disease: a collaborative project of medical students and faculty, 5th ed, Lippincott
706 Williams & Wilkins, 2011.
- 707 [15] V. N. Varghees, K. Ramachandran, A novel heart sound activity detection framework for automated heart sound analysis,
708 *Biomedical Signal Processing and Control* 13 (2014) 174–188. doi:10.1016/j.bspc.2014.05.002.
- 709 [16] S. Ismail, I. Siddiqi, U. Akram, Localization and classification of heart beats in phonocardiography signals—a compre-
710 hensive review, *EURASIP Journal on Advances in Signal Processing* 2018 (1) (2018) 1–27. doi:10.1186/s13634-018-0545-9.
- 711 [17] T.-E. Chen, S.-I. Yang, L.-T. Ho, K.-H. Tsai, Y.-H. Chen, Y.-F. Chang, Y.-H. Lai, S.-S. Wang, Y. Tsao, C.-C. Wu, S1
712 and s2 heart sound recognition using deep neural networks, *IEEE Transactions on Biomedical Engineering* 64 (2) (2017)
713 372–380. doi:10.1109/TBME.2016.2559800.
- 714 [18] J. De La Torre Cruz, F. J. Cañadas Quesada, N. Ruiz Reyes, P. Vera Candeas, J. J. Carabias Orti, Wheezing sound
715 separation based on informed inter-segment non-negative matrix partial co-factorization, *Sensors* 20 (9) (2020). doi:
716 10.3390/s20092679.
- 717 [19] P. Bentley, G. Nordehn, M. Coimbra, S. Mannor, The PASCAL Classifying Heart Sounds Challenge 2011 (CHSC2011)
718 Results, <http://www.peterjbentley.com/heartchallenge/index.html>.
- 719 [20] H. Tang, T. Li, T. Qiu, Y. Park, Segmentation of heart sounds based on dynamic clustering, *Biomedical Signal Processing*
720 *and Control* 7 (5) (2012) 509–516. doi:10.1016/j.bspc.2011.09.002.
- 721 [21] W. Zhang, J. Han, S. Deng, Abnormal heart sound detection using temporal quasi-periodic features and long short-term
722 memory without segmentation, *Biomedical Signal Processing and Control* 53 (2019) 101560. doi:10.1016/j.bspc.2019.
723 101560.
- 724 [22] A. A. Sepeshri, A. Gharehbaghi, T. Dutoit, A. Kocharian, A. Kiani, A novel method for pediatric heart sound segmentation
725 without using the ecg, *Computer Methods and Programs in Biomedicine* 99 (1) (2010) 43–48. doi:10.1016/j.cmpb.2009.
726 10.006.
- 727 [23] S. Banerjee, M. Mishra, A. Mukherjee, Segmentation and detection of first and second heart sounds (s1 and s2) using
728 variational mode decomposition, in: 2016 IEEE EMBS Conference on Biomedical Engineering and Sciences (IECBES),
729 2016, pp. 565–570. doi:10.1109/IECBES.2016.7843513.
- 730 [24] V. Nivitha Varghees, K. I. Ramachandran, Effective heart sound segmentation and murmur classification using empirical
731 wavelet transform and instantaneous phase for electronic stethoscope, *IEEE Sensors Journal* 17 (12) (2017) 3861–3872.
732 doi:10.1109/JSEN.2017.2694970.
- 733 [25] S. Das, S. Pal, M. Mitra, Acoustic feature based unsupervised approach of heart sound event detection, *Computers in*
734 *Biology and Medicine* 126 (2020) 103990. doi:10.1016/j.combiomed.2020.103990.
- 735 [26] M. Mustafa, G. Abdalla, S. Manimurugan, A. R. Alharbi, Detection of heartbeat sounds arrhythmia using automatic
736 spectral methods and cardiac auscultatory, *The Journal of Supercomputing* 76 (8) (2020) 5899–5922. doi:10.1007/
737 s11227-019-03062-7.
- 738 [27] N. Baghel, M. K. Dutta, R. Burget, Automatic diagnosis of multiple cardiac diseases from pcg signals using convolutional
739 neural network, *Computer Methods and Programs in Biomedicine* 197 (2020) 105750. doi:10.1016/j.cmpb.2020.105750.
- 740 [28] S. L. Oh, V. Jahmunah, C. P. Ooi, R.-S. Tan, E. J. Ciaccio, T. Yamakawa, M. Tanabe, M. Kobayashi, U. Rajendra
741 Acharya, Classification of heart sound signals using a novel deep wavenet model, *Computer Methods and Programs in*
742 *Biomedicine* 196 (2020) 105604. doi:10.1016/j.cmpb.2020.105604.
- 743 [29] M. Alkhodari, L. Fraiwan, Convolutional and recurrent neural networks for the detection of valvular heart diseases in
744 phonocardiogram recordings, *Computer Methods and Programs in Biomedicine* 200 (2021) 105940. doi:10.1016/j.cmpb.
745 2021.105940.
- 746 [30] J. H. McDermott, D. Wroblewski, A. J. Oxenham, Recovering sound sources from embedded repetition, *Proceedings of the*
747 *National Academy of Sciences* 108 (3) (2011) 1188–1193. doi:10.1073/pnas.1004765108.

- 748 [31] V. G. Rajendran, N. S. Harper, K. H. A. Abdel-Latif, J. W. H. Schnupp, Rhythm facilitates the detection of repeating
749 sound patterns, *Frontiers in Neuroscience* 10 (2016) 9. doi:10.3389/fnins.2016.00009.
- 750 [32] M. Kim, J. Yoo, K. Kang, S. Choi, Nonnegative matrix partial co-factorization for spectral and temporal drum source
751 separation, *IEEE Journal of Selected Topics in Signal Processing* 5 (6) (2011) 1192–1204. doi:10.1109/JSTSP.2011.
752 2158803.
- 753 [33] Z. Rafii, B. Pardo, Music/voice separation using the similarity matrix., in: 13th ISMIR, 2012, pp. 583–588.
- 754 [34] Z. Rafii, B. Pardo, Repeating pattern extraction technique (repet): A simple method for music/voice separation, *IEEE*
755 *Transactions on Audio, Speech, and Language Processing* 21 (1) (2013) 73–84. doi:10.1109/TASL.2012.2213249.
- 756 [35] J. Varghese, S. Subash, N. Tairan, Fourier transform-based windowed adaptive switching minimum filter for reducing
757 periodic noise from digital images, *IET Image Processing* 10 (9) (2016) 646–656. doi:10.1049/iet-ipr.2015.0750.
- 758 [36] F. Canadas-Quesada, N. Ruiz-Reyes, J. Carabias-Orti, P. Vera-Candeas, J. Fuertes-Garcia, A non-negative matrix fac-
759 torization approach based on spectro-temporal clustering to extract heart sounds, *Applied Acoustics* 125 (2017) 7–19.
760 doi:10.1016/j.apacoust.2017.04.005.
- 761 [37] J. Foote, Visualizing music and audio using self-similarity, in: *Proceedings of the Seventh ACM International Conference*
762 *on Multimedia (Part 1)*, MULTIMEDIA '99, Association for Computing Machinery, New York, NY, USA, 1999, p. 77–80.
763 doi:10.1145/319463.319472.
- 764 [38] E. F. Gomes, P. J. Bentley, E. Pereira, M. T. Coimbra, Y. Deng, Classifying heart sounds - approaches to the pascal
765 challenge, in: *HEALTHINF*, 2013.
- 766 [39] V. K. Shivhare, S. N. Sharma, D. K. Shakya, Detection of heart sounds s1 and s2 using optimized s-transform and back
767 — propagation algorithm, in: 2015 IEEE Bombay Section Symposium (IBSS), 2015, pp. 1–6. doi:10.1109/IBSS.2015.
768 7456661.
- 769 [40] D. Boutana, M. Benidir, B. Barkat, Segmentation and identification of some pathological phonocardiogram signals using
770 time-frequency analysis, *IET signal processing* 5 (6) (2011) 527–537. doi:10.1049/iet-spr.2010.0013.
- 771 [41] L. Avendano-Valencia, J. Godino-Llorente, M. Blanco-Velasco, G. Castellanos-Dominguez, Feature extraction from para-
772 metric time-frequency representations for heart murmur detection, *Annals of Biomedical Engineering* 38 (8) (2010) 2716–
773 2732. doi:10.1007/s10439-010-0077-4.
- 774 [42] I. Maglogiannis, E. Loukis, E. Zafiroopoulos, A. Stasis, Support vectors machine-based identification of heart valve diseases
775 using heart sounds, *Computer Methods and Programs in Biomedicine* 95 (1) (2009) 47–61. doi:10.1016/j.cmpb.2009.
776 01.003.
- 777 [43] A. Moukadem, A. Dieterlen, N. Hueber, C. Brandt, A robust heart sounds segmentation module based on s-transform,
778 *Biomedical Signal Processing and Control* 8 (3) (2013) 273–281. doi:10.1016/j.bspc.2012.11.008.
- 779 [44] Z. Dokur, T. Ölmez, Heart sound classification using wavelet transform and incremental self-organizing map, *Digital Signal*
780 *Processing* 18 (6) (2008) 951–959. doi:10.1016/j.dsp.2008.06.001.
- 781 [45] K. Ferenc, H. Csaba, B. Á d á m, H. G á bor, Extended noninvasive fetal monitoring by detailed analysis of data measured with
782 phonocardiography, *IEEE Transactions on Biomedical Engineering* 58 (1) (2011) 64–70. doi:10.1109/TBME.2010.2071871.
- 783 [46] V. Nivitha Varghees, K. I. Ramachandran, Effective heart sound segmentation and murmur classification using empirical
784 wavelet transform and instantaneous phase for electronic stethoscope, *IEEE Sensors Journal* 17 (12) (2017) 3861–3872.
785 doi:10.1109/JSEN.2017.2694970.
- 786 [47] S. Chauhan, P. Wang, C. Sing Lim, V. Anantharaman, A computer-aided mfcc-based hmm system for automatic auscult-
787 ation, *Computers in Biology and Medicine* 38 (2) (2008) 221–233. doi:10.1016/j.combiomed.2007.10.006.
- 788 [48] H. Naseri, M. Homaeinezhad, Detection and boundary identification of phonocardiogram sounds using an expert frequency-
789 energy based metric, *Annals of biomedical engineering* 41 (2) (2013) 279–292. doi:10.1007/s10439-012-0645-x.
- 790 [49] F. Chakir, A. Jilbab, C. Nacir, A. Hammouch, A. Hajjam El Hassani, Detection and identification algorithm of the s1
791 and s2 heart sounds, in: 2016 International Conference on Electrical and Information Technologies (ICEIT), 2016, pp.
792 418–420. doi:10.1109/EITech.2016.7519633.
- 793 [50] I. Turkoglu, A. Arslan, E. Ilkay, An expert system for diagnosis of the heart valve diseases, *Expert Systems with Appli-*
794 *cations* 23 (3) (2002) 229–236. doi:10.1016/S0957-4174(02)00042-8.
- 795 [51] S. Ari, K. Hembam, G. Saha, Detection of cardiac abnormality from pcg signal using lms based least square svm classifier,
796 *Expert Systems with Applications* 37 (12) (2010) 8019–8026. doi:10.1016/j.eswa.2010.05.088.
- 797 [52] P. Sedighian, A. W. Subudhi, F. Scalzo, S. Asgari, Pediatric heart sound segmentation using hidden markov model, in:
798 2014 36th Annual International Conference of the IEEE Engineering in Medicine and Biology Society, 2014, pp. 5490–5493.
799 doi:10.1109/EMBC.2014.6944869.
- 800 [53] D. B. Springer, L. Tarassenko, G. D. Clifford, Logistic regression-hsmm-based heart sound segmentation, *IEEE Transac-*
801 *tions on Biomedical Engineering* 63 (4) (2016) 822–832. doi:10.1109/TBME.2015.2475278.
- 802 [54] C. D. Papadaniil, L. J. Hadjileontiadis, Efficient heart sound segmentation and extraction using ensemble empirical
803 mode decomposition and kurtosis features, *IEEE Journal of Biomedical and Health Informatics* 18 (4) (2014) 1138–1152.
804 doi:10.1109/JBHI.2013.2294399.
- 805 [55] A. H. Salman, N. Ahmadi, R. Mengko, A. Z. Langi, T. L. Mengko, Empirical mode decomposition (emd) based denoising
806 method for heart sound signal and its performance analysis., *International Journal of Electrical & Computer Engineering*
807 (2088-8708) 6 (5) (2016). doi:10.11591/ijece.v6i5.pp2197-2204.
- 808 [56] C. N. Gupta, R. Palaniappan, S. Swaminathan, S. M. Krishnan, Neural network classification of homomorphic segmented
809 heart sounds, *Applied Soft Computing* 7 (1) (2007) 286–297. doi:10.1016/j.asoc.2005.06.006.
- 810 [57] Y. Yin, K. Ma, M. Liu, Temporal convolutional network connected with an anti-arrhythmia hidden semi-markov model
811 for heart sound segmentation, *Applied Sciences* 10 (20) (2020). doi:10.3390/app10207049.
- 812 [58] Trapezoidal numerical integration (trapz function of MATLAB software), <https://es.mathworks.com/help/matlab/ref/>

- 813 trapz.html, online. Accessed: 2021-12-20 (2021).
- 814 [59] V. G. Sujadevi, K. P. Soman, R. Vinayakumar, A. U. P. Sankar, Deep models for phonocardiography (pcg) classification, in:
815 2017 International Conference on Intelligent Communication and Computational Techniques (ICCT), 2017, pp. 211–216.
816 doi:10.1109/INTELCCT.2017.8324047.
- 817 [60] R. Banerjee, A. Ghose, A semi-supervised approach for identifying abnormal heart sounds using variational autoencoder,
818 in: ICASSP 2020 - 2020 IEEE International Conference on Acoustics, Speech and Signal Processing (ICASSP), 2020, pp.
819 1249–1253. doi:10.1109/ICASSP40776.2020.9054632.
- 820 [61] J. H. Oliveira, F. Renna, P. Costa, D. Nogueira, C. Oliveira, C. Ferreira, A. Jorge, S. Mattos, T. Hatem, T. Tavares,
821 A. Elola, A. Rad, R. Sameni, G. D. Clifford, M. T. Coimbra, The circor digiscope dataset: From murmur detection to
822 murmur classification, *IEEE Journal of Biomedical and Health Informatics* (2021). doi:10.1109/JBHI.2021.3137048.
- 823 [62] J. Oliveira, F. Renna, P. Costa, M. Nogueira, A. C. Oliveira, A. Elola, C. Ferreira, A. Jorge, R. A. Bahrami, M. Reyna,
824 R. Sameni, G. Clifford, C. Miguel, The circor digiscope phonocardiogram dataset (version 1.0.1), *PhysioNet* (2022).
825 doi:10.13026/7bkn-d780.